MRI ASSESSMENT OF LOCAL DEFORMATIONS ALONG HUMAN MEDIAL GASTROCNEMIUS MUSCLE FIBERS ON SUBMAXIMAL PLANTARFLEXION ACTIVITY

by

Agah Karakuzu

B.Sc., Biomedical Engineering, Erciyes University, 2013

Submitted to the Institute of Biomedical Engineering

in partial fulfillment of the requirements

for the degree of

Master of Science

in

Biomedical Engineering

Boğaziçi University

2015

MRI ASSESSMENT OF LOCAL DEFORMATIONS ALONG HUMAN MEDIAL GASTROCNEMIUS MUSCLE FIBERS ON SUBMAXIMAL PLANTARFLEXION ACTIVITY

APPROVED BY:

Assoc. Prof. Dr. Can A. Yücesoy . . . .

(Thesis Advisor)

Assoc. Prof. Dr. Burak Acar . . . .

Assist. Prof. Dr. Esin Öztürk Işık . . . .

DATE OF APPROVAL: 11 June 2015

ACKNOWLEDGMENTS

ABSTRACT

MRI ASSESSMENT OF LOCAL DEFORMATIONS ALONG HUMAN MEDIAL GASTROCNEMIUS MUSCLE FIBERS ON SUBMAXIMAL PLANTARFLEXION ACTIVITY

Comprehensive understanding of the mechanical interactions between skeletal muscles within their integral system of connective tissues requires simultaneous quantification of the architecture, force and deformation during *in-vivo* muscle action. For that purpose, magnetic resonance imaging (MRI) along with nonrigid Demons registration were applied together to quantify 3D local deformations. Additionally, diffusion tensor imaging (DTI) was utilized to reconstruct 3D muscle fiber architecture. Use of such multi-method approach and specifically designed experimental equipments together enabled the *in-vivo* quantification of local strains along the orientation of the skeletal muscle fibers occurring due to activation. The specific goal of this study was to test the hypothesis that 15% of maximal voluntary isometric contraction (MVIC) of sustained plantar flexion results in a serial strain distribution along the muscle fibers of medial gastrocnemius (GM) of female subjects (n=5). Results indicate that considerable local lengthening and shortening occurs simultaneously within individual GM tracts (e.g. from 12.4% shortening up to 36.7% lengthening within a single tract) through the muscle.The hypothesis is therefore confirmed. Moreover, a parallel distribution was also found to be heterogeneous. Such findings are the characteristic indications of myofascial force transmission effects that highlights the interdependent mechanical functionality of skeletal muscles. To our knowledge, this is the first study in the literature that enables the evaluation of *in-vivo* deformations caused by submaximal isometric contraction with respect to the muscle fiber orientations of GM. Such experimental work therefore is expected to lay the groundwork for the investigation of *in-vivo* myofascial force transmission effects on clinical applications like botulinum toxin treatment and tendon transfer surgery.

Keywords: MRI, tractography, gastrocnemius, *in-vivo*, myofascial force transmission.

ÖZET

MRG YÖNTEMİ KULLANILARAK SUBMAKSİMAL PLANTAR FLEKSİYON AKTİVİTESİ SONUCUNDA ORTAYA ÇIKAN LOKAL DEFORMASYONLARIN İNSAN MEDİAL GASTROCNEMİUS KASI FİBERLERİ BOYUNCA DEĞERLENDİRİLMESİ

Kaslar arasındaki mekaniksel etkileşimleri çevreleri dahilinde kapsamlı bir şekilde değerlendirmek için; kaslara ait mimarinin, kuvvetin ve deformasyonun eş zamanlı olarak hesaplanması gereklidir. Bu sebeple, 3B yerel deformasyonları elde edebilmek için Manyetik Rezonans Görüntüleme (MRG) ve Demons imge çakıştırma yöntemleri kullanıldı. Dahası, kas fiber mimarisi difüzyon tensör görüntüleme (DTG) ile belirlendi. Bu çok yöntemli yaklaşım ve özel olarak tasarlanan deneysel ekipmanlar, aktivasyon sonucunda ortaya çıkan yerel şekil değiştirme bilgisinin kas fiberleri boyunca nicellenmesini mümkün kıldı. Bu çalışmanın hedefi, maksimum istemli kasılmanın %15'i ile gerçekleştirilen izometrik plantar fleksiyon aktivitesi sonucunda medial gastrocnemius (GM) fiberleri boyunca seri gerinim dağılımın gözlemleneceği hipotezini 5 kadın denek üzerinde test etmektir. Elde edilen sonuçlar, fiber yönü yerel uzama ve kısalmaların aynı kas fiberleri içinde eş zamanlı olarak ortaya çıktığını (örn. tek bir fiberde seri dağılım %12.4 kısalma ve %36.7 uzama aralığındadır) gösterdi ve hipotezi doğruladı. Dahası, sonuçlarımız paralel dağılımın da heterojenite gösterdiğini ortaya koymaktadır. Bu bulgular miyobağdokusal kuvvet iletiminin karakteristik bir göstergesi olmakla birlikte, iskelet kaslarının mekaniksel açıdan birbirlerinden bağımsız olmadığını vurgulamaktadır. Bilgimiz dahilinde, bu çalışma düşük kuvvetle gerçekleştirilen izometrik istemli kasılma sonucunda ortaya çıkan deformasyonu kas fiberleri yönünde nicellemeyi mümkün kılan ilk çalışmadır.Bu çalışma miyobağdokusal kuvvet iletiminin botulinum toxin uygulaması veya tendon gevşetme operasyonları gibi klinik uygulamalar üzerine olan etkilerinin canlı ortamda araştırılması için zemin oluşturmaktadır.

Anahtar Sözcükler: MRI, traktografi, *in-vivo*, miyobağdokusal kuvvet iletimi

TABLE OF CONTENTS

LIST OF FIGURES

LIST OF TABLES

LIST OF SYMBOLS

T	Tesla
E	Strain tensor
$P(X)$	Undeformed configuration point
$P(x)$	Deformed configuration point
$\vec{u}$	Displacement vector
∇u	Displacement gradient
F	Deformation gradient
I	3×3 Identity matrix
$\bar{E}$	Interpolated strain tensor
SC	Strain coefficient
$\vec{t}$	Normalized tangent vector
W_i	Normalized weight at i^{th} voxel
E_i	Strain tensor at i^{th} voxel

LIST OF ABBREVIATIONS

MRI	Magnetic Resonance Imaging
DTI	Diffusion Tensor Imaging
MR	Magnetic Resonance
DT	Diffusion Tensor
IQR	Inter-Quartile Range
MVIC	Maximal Voluntary Isometric Contraction
FOV	Field of View
ROI	Region of Interest
DWI	Diffusion Weighted Images
GM	Medial Gastrocnemius Muscle
GL	Lateral Gastrocnemius Muscle
GM	Medial Gastrocnemius Muscle
GAS	Gastrocnemius Muscle
SOL	Soleus Muscle
TA	Tibialis Anterior Muscle
EDL	Extensor Digitorum Longus Muscle
EHL	Extensor Hallicus Longus Muscle
FA	Fractional Anisotropy
DENSE	Displacement Encoding With Stimulated Echoes
HARP	Harmonic Phase MRI
SENC	Strain-Encoded MRI
TMRI	Spin Tagging MRI

1. INTRODUCTION

1.1 Skeletal Muscle

1.1.1 Hierarchical Structure of the Skeletal Muscle

Skeletal muscle is responsible for vertebrate locomotion and posture. It is composed of myocytes (muscle fibers) and connective tissues. Muscle fibers are one of the largest cells in human body with hundred microns in diameter and few centimeters in length. Each muscle fiber is composed of myofibrils. Myofibrils are composed of arrangements of myofilaments repeated in units called a sarcomere. Sarcomeres are approximately from 2.25 μm to 2.50 μm in length and arranged in series within muscle fibers, which in turn forms a striated pattern. Sarcomeres are the smallest functioning mechanical unit, which acts like muscle. Their activation is explained by sliding filament theory [1].

Connective tissues are basically composed of collagen and found at different levels within the skeletal muscle. The outermost layer is constituted by a strong connective tissue that surrounds the whole muscle called superficial fascia. Epimysium, also called deep fascia, covers the whole muscle just beneath the fascia. Muscle fibers together form the fascicles that are surrounded by perimysium. Epimysium contains nerves and blood vessels and constitutes a path to let them reach to the inner parts of the muscle. Each muscle fiber has a cell membrane called the sarcolemma and muscle fibers are also surrounded by endomysium. Connective tissues of skeletal muscle show interconnectivity and merge together to form aponeuroses and tendons towards the distal and proximal endings of the muscle (Figure 1.1).
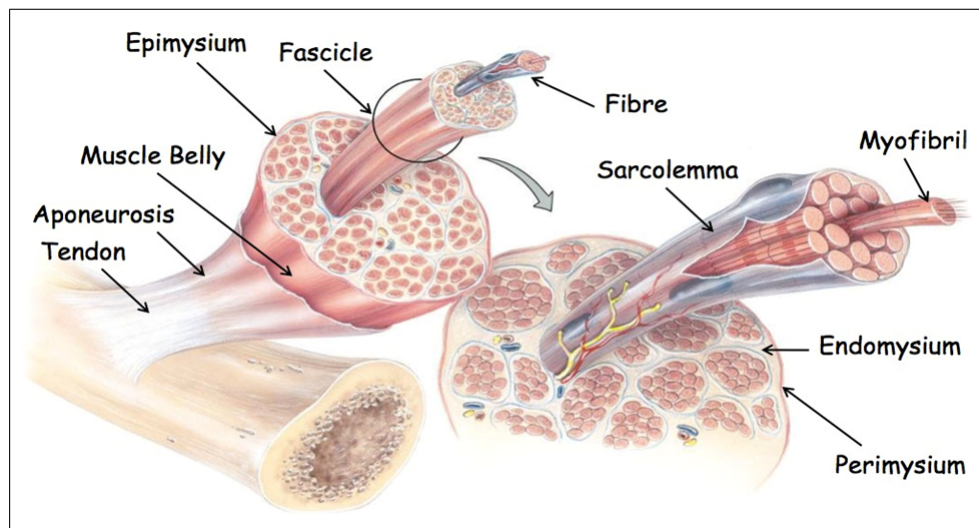
Figure 1.1 Hierarchial organization of the skeletal muscle [2].

1.1.2 Contraction of the Skeletal Muscle

Skeletal muscle contraction occurs as a result of a voluntary effort that stems from the brain. In order to initiate a contraction, an action potential from the central nervous system must be conveyed to the neuromuscular junctions i.e. the region where motor neuron innervates to the muscle fibers. A motor neuron may be in contact with a couple or bunch of muscle fibers at the neuromuscular junctions. These functional units composed of several muscle fibers and motor neurons termed as motor units. In a motor unit, number of fibers per neuron determines the precision of the movement performed by that muscle, also known as motor unit ratio. For example medial gastrocnemius (GM), which is a plantar flexor muscle, contains approximately a million of muscle fibers and 600 alpha motor axons, whereas lateral rectus muscle, which is one of the muscles responsible for eye movement, contains 22 thousand muscle fibers and 4150 alpha motor neurons [3].

Skeletal muscle contractions are generally divided in two groups according to the intensity of the stimulation. Twitch contraction identifies a short burst of stimulation with a short duration, which eventually results in a weak contraction. On the other hand, tetanic contractions occur as a result of long-duration stimulus and let the muscle reach its peak force. Another classification of the skeletal muscle contraction is made on

the basis of the length changes and force levels (i) concentric contraction, (ii) eccentric contraction, (iii) isometric contraction, (iv) isotonic contraction, and (iv) isokinetic contraction.

1.2   Musculoskeletal Biomechanics Imaging

A comprehensive analysis of skeletal muscle mechanics using imaging modalities requires a collaborative work with the researchers from different disciplines. It is a challenging task to implement methods from various disciplines and combining them properly to investigate the hypothesis in the focus of interest. However, beyond these application-oriented difficulties, imaging methods provide favorable tools to investigate mechanical characteristics of the skeletal muscles since they allow researchers to evaluate *in-vivo* interactions within the integral system of the organization.

From the biomechanical perspective, assessment of the *in-vivo* length changes occurred due to various changes in the muscle-joint configurations or even due to contraction has a key importance for understanding functional properties of that muscle. Because, the length in which sarcomeres from various locations that show activity is a major determinant of the force production capacity of the skeletal muscle and the joint range of motion [4]. In addition to the length changes, evaluation of the architectural parameters e.g. pennation angle, fascicle lengths and fiber orientations also provide insightful information about functionality. Thanks to ground-braking developments in the field of medical imaging, much research in the last decades has focused on evaluating *in-vivo* length changes and architectural properties of human skeletal muscles using imaging methods, especially ultrasound and magnetic resonance imaging (MRI).

1.2.1   Ultrasound in Musculoskeletal Biomechanics

Using ultrasonography, Masamitsu et al. [5] measured fascicle and tendon length changes and also changes in the structural parameters of tibialis anterior (TA) mus-

cle during isometric dorsi flexion. They drew the conclusion that mechanical work is generated by the shortening of the muscle fibers and a portion of generated force is absorbed by tendinious structures and caused them to elongate. Within the same year, Kawakami's group [6] utilized ultrasonography to investigate architectural and functional changes in triceps surae muscles during MVIC of plantar flexion with respect to the altered knee and ankle angles. They concluded that fascicle shortening occurs more considerably at longer fascicle lengths and also indicated that emerged differences in lengths and pennations due to different joint configurations or contraction may be related to force production potentials of the active components and the elastic characteristics of the tendinous tissues. In a more recent study, Lichtwark et al. performed the measurement of the length changes along the human gastrocnemius (GAS) during human locomotion using sonography [7]. They asserted that fascicles of GM act similarly at each site during walking and running by extrapolating the average fascicle length changes across the length of the muscle from the fascicles located on the intermediate region. There are also other studies in the literature that focus on the investigation of the skeletal muscle-tendon characteristics during human locomotion using ultrasonography [8, 9]. Although validity of ultrasound on estimating architectural properties of skeletal muscles using 2D data was shown across a broad range of experimental conditions [10], Rana et al. [11] pointed out that pennation angle estimations in 2D studies are highly dependent on the orientation of the scanning plane and can be different from their actual 3D values. They argued that 2D ultrasound measurements may underestimate the complex fascicle orientations especially for the muscles in which their fascicles lie along a curved surface in 3D space, which in turn results in inadequate information to describe force transmission in 3D and therefore may ignore the existence of additional force transmission pathways [12] other than myotendinous junctions.

Ultrasound is an advantageous method for researching skeletal muscle mechanics on the score of its being an affordable, fast and easy to operate. However, ultrasound gives data over a small plane. To put it another way, field of view (FOV) of the ultrasound images are restricted by the size of the probe, which in return makes it unfeasible to measure large areas of muscles simultaneously. Furthermore, when imaging a large

size muscle, it even may not be possible to image whole continuation of the fascicles from origin to the insertion [13]. Besides, experienced sonographer dependency is required for imaging fascicles and tendons properly, which eventually makes the image acquisition user dependent. Penetration depth of the ultrasound probe constitutes another limitation to image deep muscles. In addition, there is a compromise between the spatial resolution and the penetration depth.

1.2.2 MRI in Musculoskeletal Biomechanics

MRI is a non-invasive and non-ionizing imaging method that makes it possible to acquire images with different features, multiplanar capability and supreme soft-tissue contrast. Thanks to these promising features, MRI has been established as one of the most purposive tools for the assessment of the musculoskeletal system. Utilization of the advanced kinematic MRI sequences enables tracking the *in-vivo* movement of the tissues within the FOV. These methods are i) velocity encoded phase contrast MRI (PC-MRI), ii) pulse field gradient based MRI methods (HARP and DENSE), iii) spin tagging MRI (TMRI) and iv) strain encoding imaging (SENC). Since these methods enable the quantification of the *in-vivo* displacement and even strain fields, they have been being widely utilized for musculoskeletal biomechanics applications.

Using PC-MRI, TMRI and morphological MRI method in combination, Kinugasa et al. [14] examined the GM muscle during 20% and 40% of MVIC plantarflexion. It is concluded from the quantified strain and displacement information that strain distribution occurs non-uniformly along the both aponeurosis of the GM and both of the aponeuroses moves in the proximal direction as a result of the lower to moderate isometric plantarflexion. Shin's group quantified GM muscle and aponeurosis deformation during active and passive eccentric movements of the plantarflexors using PC-MRI [15]. Results from this study also indicated that significant intramuscular heterogeneity occurs through the proximodistal axis of GM. PC-MRI technique was also applied by Blemker et al. [16] and Pappas [17], and they both concluded that non-uniform strains occur in the human biceps brachii during elbow flexion. Dynamic MRI methods were

not only performed on healthy subjects but also were used for the postoperative evaluation of the rectus femoris muscle after tendon transfer surgery [18]. The main purpose of the surgery was to convert the rectus femoris from a knee extensor to a knee flexor. However, PC-MRI results provided compelling evidence that target muscle does not move in the same direction with knee flexors. On one hand this case shows that how dynamic MRI methods may offer an understanding of the post-operational effects of the remedial surgery; on the other hand points to the necessity of a comprehensive approach to the evaluation of intermuscular interactions for a sufficient clarification of the results.

All of these reviewed MRI studies report that both myofibers and tendinous tissues exhibits a complex mechanical behavior during various activation within their surroundings. Although these findings from the literature constitute a clear discrepancy with the classical presumption that muscle fibers undergo uniform shortening throughout the muscle as a result of activation, few attempts have been made to address the underlying reasons of such heterogeneity in the length changes.

Quantification of the *in-vivo* strain, even expressed in terms of an outside coordinate system, may provide useful information for the inference of the mechanical behavior of the skeletal muscles. However, it is widely known that sarcomeres are arranged in series within the muscle fibers, hence deformation in the direction of the muscle fibers provide a physiologically more relevant information regarding the *in-vivo* functionality. Fortunately, MRI provides a powerful tool to determine muscle fiber directions *in-vivo*: diffusion tensor imaging (DTI).

DTI is an MRI method that makes the use of the susceptibility of the diffusion of the water molecules to the local environment in tissues. Cell membranes and other organized microstructures restrict the the movement of the water molecules in a certain direction. This phenomenon also known as anisotropic diffusion. When such behavior of water molecules considered within the skeletal muscles, principal direction of the diffusion identifies the direction along the muscle fibers [19]. It was reported in the literature that when DTI applied to the skeletal muscles, principal diffusion direction

aligns with the predominant orientation of the myofibers [20], which in turn enables the tracking of the muscle fibers by using tractography methods. Tractography is a computational process in which fibrous architecture is constructed and visualized using diffusion weighted data. Repeatability of the skeletal muscle fiber tracking using DTI was also reported [21]. Most research done to date for the purpose of evaluating the structural characteristics and the diffusion properties of the skeletal muscles using DTI tractograpghy [22–26].

Despite the provided advantages, few studies in the literature have focused on the combined utilization of DTI and musculoskeletal MRI methods in order to evaulate *in-vivo* deformations in the direction of the muscle fibers. Englund et. al [27] evaluated voxel-wise strain tensors due to submaximal isometric contraction of tibialis anterior (TA) with respect to the muscle fiber direction using DTI and TMRI together. However, they did not calculated the fiber direction strains straightforwardly. Instead, they used diffusion tensors to compare its direction with the direction of positive and negative principal strains. They concluded that length changes occurs in deep compartment of TA with a greater magnitude than those occurred in superficial compartment, which consequently points to a heterogeneity in the strain distribution. Another conclusion from this study was that shortening direction deviated from the direction of the local muscle fiber orientations. In another study, Felton et. al [28] utilized PC-MRI for local strains and DTI for mesoscale fiber orientations of tongue during swallowing. Combining these informations, they computed the strain rate in the direction of myofiber tracts. They concluded that complex lingual deformations occur due to the interactions of the intrinsic and extrinsic muscles responsible together for swallowing. Authors also pointed out the limitation that fiber tract imaging performed under passive state, whereas strain rate quantification was performed during a dynamic contraction; which in return may underestimate variation in the muscle fiber architecture.

In conclusion, MRI attracts a widespread attention for the biomechanical studies concerning the *in-vivo* skeletal muscle function; since it has the advantages of having a high spatial resolution, multiplanar imaging capability without subject repositioning and providing a large FOV in a non-ionizing and non-invasive manner. Apart

from these, MRI also provides specialized tools that are suited for *in-vivo* soft tissue deformation analysis and for muscle fiber imaging. On the other hand MRI is an expensive method and it takes relatively longer to acquire images compared with the other imaging modalities e.g., ultrasound. Besides, MRI makes it challenging to design experimental setups on account of the fact that working environment is restricted by the diameter of the magnet bore and strong magnetic field requires the utilization of MRI compatible equipments. Despite all, it is the most efficient method to study heterogeneous muscle fascicle length changes for a better understanding of the complex mechanical interactions within the integral system of the skeletal muscles.

Evidently, studies from the literature have pointed out that MRI analyses reveal the complex functional behavior of the skeletal muscles *in-vivo*. However, attributed reasons to most of these results may be oversimplified for a comprehensive understanding. Apparently, the classical approach to the muscle mechanics, which presumes that the skeletal muscles are independent actuators and myotendinous junctions are the exclusive sites for the force transmission, is not representative for the explanation of these findings. On the other hand, structural and mechanical complexities within the muscle e.g. complex muscle-tendon architecture [17], variation in fascicle lengths and curvature of the fascicles [16] may not solely address to the presence of such heterogeneous length changes. Thus, an alternative and more exhaustive approach is required; myofascial force transmission [12, 29–31].

1.3   Force Transmission Mechanisms

1.3.1   Myotendinous Force Transmission

The connection sites of the muscle fibers to the tendons are called as myotendinous connections. Connective tissues of skeletal muscle shows a continuity and combine together to form aponeurosis and tendons towards the distal and proximal endings of the muscles. Tendons are specialized structures to transmit force generated in the muscle to the tendons. Following this, tendons transmit the force to the bone and

to the joints [32]. Importance of such myotendinous force transmission is obvious. Without the transmission of the force via these channels to the bony structures, movement of the limbs would not be possible. Supposedly, on account of their being well suited to transmit force, myotendinous junctions are presumed to be exclusive sites for force transmission [33]. Such assumption made by the classical point of view implicitly implies that skeletal muscles are isolated from each other.

In consequence, upon the presumption of the classical point view it is feasible to infer that skeletal muscles are considered to be independent actuators, proximal and distal tendon forces are equal and length-force characteristics are unique properties of skeletal muscles [12].

1.3.2 Myofascial Force Transmission

In the most general sense, myofascial force transmission refers to the force transmission between muscle and its surroundings [34]. Existence of such force transmission therefore indicates the presence of additional structures other than myotendinous junctions that have the ability to transmit force. The extracellular matrix can be represented as a 3D set of endomysial tunnels in which muscle fibers operate [35]. Muscle fibers are linked to this extracellular matrix lattice via transsarcolemmal connections along their full peripheral surface. Evidence in the literature shows that these multimolecular structures have the ability to transmit force in a crosswise direction. Following the partial isolation of a frog myofiber, force measurements from the partially left intact surroundings pointed out that force generated by activation is transmitted laterally [36]. Such force transmission that takes places in between of the muscle fibers and the extracellular matrix is termed as intramuscular myofascial force transmission.

Numerous skeletal muscle fibers function within a hierarchically organized integral system of the extracellular matrix. Moreover, extracellular connective tissue stroma is continuous for the all level of organizations i.e. from endomysium to the superficial fascia. Reasonably, awareness of the relation between such continuity and the

intramuscular force transmission makes it plausible to infer that force transmission also occurs within the higher level of organizations. Force transmission over these continuous collagenous structures is termed as intermuscular myofascial force transmission In addition to this direct collagenous linkages between the adjacent muscles [37] neurovascular tracts also contribute to this connection indirectly [38]. Connections between the neurovascular tracts and compartmental boundaries e.g. intermuscular septa, periost and compartmental fascia also provide a force transmission pathway. These connections, which link muscular and non-muscular structures, are termed as extramuscular connections that enables extramuscular myofascial force transmission.

Studies in the literature, which are specifically suited to research the influences of the myofascial force transmission on skeletal muscle mechanics, addressed to the essential effects of this novel approach on muscular mechanics: (i) unequal proximo-distal forces. *In-situ* animal experiments highlighted the difference in the exerted muscle forces at the origin and insertion. For instance, keeping rat anterior crural compartment muscles (extensor digitorum longus (EDL), TA and extensor hallucis longus (EHL)) intact , Huijing et al. [39] measured exerted forces at proximal and distal tendons of EDL muscle with respect to different lengths and conditions, upon the simultaneous maximal stimulation of all muscles in the compartment. They reported uneven proximal and distal EDL forces for any length of the EDL and primarily ascribed these results to extramuscular myofascial force transmission. Another study, however with different experimental conditions, also reported proximo-distal force differences on rat EDL muscle and attributed this finding to the intermuscular force transmission [40] (ii) muscle relative position as a major co-determinant of muscle force. It was shown that by keeping surrounding structures intact, changing the relative position of an isometric skeletal muscle with respect to these structures augments the effect of myofascial force transmission and yields a higher proximo-distal force difference on rat EDL muscle [41] (iii) muscle length-force characteristics are not unique properties of skeletal muscles. A previous study focused on the effect of epimuscular connections between rat EDL and EHL synergistic muscles by Yucesoy et al. [37] reported that although its muscle range of force exertion remained constant; upon removal of the EDL muscle, length-force characteristics of EHL changed significantly. Consequently, they highlighted the

presence of sufficient stiffness of the epimuscular pathways to enable inter- and extra-muscular force transmission. (iv) major sarcomere length heterogeneity. Yucesoy et al. [42] developed a finite element model in which skeletal muscle is divided into two domains: (i) intracellular domain and (ii) extracellular matrix domain. Furthermore, these two domains were linked elastically to represent attachment of the muscle fibers to the extracellular connective tissue stroma [35], which in turn enabled the evaluation of force transmission between these domains. Using this model model they reported that serial strain distribution occurs heterogeneously within the same individual muscle fiber by virtue of intermuscular and extramuscular connections [43]. Such heterogeneous distribution within muscle fibers suggests that presence of myofascial loads not only affect force transmission mechanisms, but also have substantial functional effects on the mechanical characteristics of skeletal muscle e.g. alternations in muscle force production characteristics. For a detailed review on myofascial force transmission the reader is referred to [12, 34].

1.4   Assessment of Myofascial Force Transmission using MRI

So far, our research group has done various researches with the intention of the assessment of the *in-vivo* effects of myofascial force transmission using MRI. Using Demons algorithm [44] Yaman et al. [45] have quantified the voxel-wise strain tensors occurred as a result of passive knee flexion while ankle kept in neutral position. This method has enabled the volumetric analysis of strain distribution, however with respect to the global coordinate system, within the triceps surae muscle and also within the other muscle compartments of human lower leg. They have reported that positive and negative local strains occurred together within the bi-articular GAS muscle. Apart from that, in spite of their global isometric conditions with respect to passive knee flexion, heteronegenous deformation has been also observed within the synergistic soleus (SOL) and within the antagonist muscle groups.These findings therefore constitutes an evidence for *in-vivo* existence of the myofascial force transmission effects and implies the mechanical inter dependency of the skeletal muscles. Next, a preliminary attempt has been made to represent *in-vivo* fiber direction deformation due to

passive knee flexion by combining voxel-wise strain quantification method based on non-rigid Demons registration with DTI, which enables the determination of principal muscle fiber orientations [46]. Remarkable local fiber direction strain heterogeneity has been reported within the synergistic, as well as antagonistic muscle groups of the lower leg. For a better representation, local deformations due to passive knee extension have been visualized on the muscle tracts of the TA [47] and GM [48] muscles. It has been concluded that passive knee extension results in serial and parallel distribution within the bi-articular GM, as well as within the TA muscle despite its globally isometric condition. An experimental method has been developed to quantify local fiber direction deformations during ankle joint motion using PC-MRI and DTI combined [49]. Preliminary findings from this study have reported that heterogeneous fiber direction strain occurs along the GM and SOL muscles during joint motion. Although it enables the quantification of the strain from a directly physiologically related information i.e. velocity of the tissues during joint motion, such method imposes some limitations: (i) volumetric strain analysis is not possible because PC-MRI restricts image acquisition to a single plane and (ii) DTI cannot be performed during joint motion, therefore localization of the fiber directions must be performed at a certain time frame.

1.5   Objective of the Study

Alongside the finite element modeling studies [4,42,43] and *in-situ* animal experiments [37,40,41,50] musculoskeletal biomechanics oriented MRI applications together with non-rigid Demons registration method provide a powerful tool for evaluating *in-vivo* effects of the myofascial force transmission. Moreover, effectiveness of Demons algorithm for such specific purpose has been shown by the publications of our research group [45,48]. Results from the studies in which DTI has been also utilized to quantify length changes in the muscle fiber direction [46–48] have been shown to be in good agreement with the results of the previous finite element studies and have addressed to the substantial effects of myofascial force transmission under passive conditions. However, little work has been done for investigation of such effects during activation using MRI [49]. On the other hand, intraoperative experiments by Ates et al. have

reported striking results that when activated alone, spastic human muscle show no abnormal mechanical behavior, but that this ceases when an antagonistic muscle is coactivated [51]. Such results have highlighted the clinical importance of the myofascial force transmission. There remains a need for MRI experiments that enable the quantification of fiber direction length changes due to *in-vivo* muscle activation.

Using and improving previously implemented MRI methods by our research group, we specifically aimed at quantifying local deformations with reference to the tracked muscle fibers of human GM muscle during 15% MVIC of sustained plantar flexion, *in-vivo*. Based on myofascial force transmission effects we hypothesized that 15% MVIC of sustained plantar flexion results in heterogeneous serial distribution along the muscle fibers of GM.

2. METHODS

2.1 Subjects

Experimental procedures were in strict agreement with the guidelines and regulations concerning human welfare and experimentation set by Turkish law and approved by a Committee on Ethics of Human Experimentation at Boğaziçi University, Istanbul. Five healthy female subjects (age=26±3year, height=162±7cm and body mass=51±5kg) volunteered for this study. Only female subjects were recruited in order to minimize inter-subject anthropometric differences (Table 2.1). Following a detailed explanation of the purpose and methodology of the experiments, the subjects gave their written informed consent.

Table 2.1
Anthropometric data for each subject.

Subject	Height (cm)	Weight (kg)	Age	Extension (°)
1	160	47	25	178
2	154	45	27	176
3	165	56	28	178
4	170	54	22	170
5	162	45	26	176

2.2 Experimental Protocol

Since experimental procedure requires subjects to maintain a certain level of contraction for a length of time during image acquisition, preliminary force measurements were performed outside of the MRI scanner. Detailed information about the experimental setups and procedures comprising both before and during MRI data acquisition is provided in this section.

2.2.1 Maximal Voluntary Isometric Contraction Measurement

Subjects were positioned on a table in prone position. The right foot was firmly fastened to a custom-built aluminum foot pedal (Figure 2.1) equipped with a strain gauge (ESIT, STCS200,Istanbul,Turkey) at an ankle angle of 90°, whereas knee joint was maintained at full extension. Care was taken not to exert undesired loads upon target muscle groups and tendons. Next, pre-gelled and self-adhesive electromyography (EMG) surface electrodes were placed on proper positions [52] in order to acquire signal simultaneously with force measurement (Biopac MP150 with DA100C, CA, USA) during plantar flexion effort from TA, SOL, GM and gastrocnemius lateralis (GL) muscles. EMG measurements were performed on these muscles since the first three of them are the primer determinant of the force generated during plantar flexion effort.
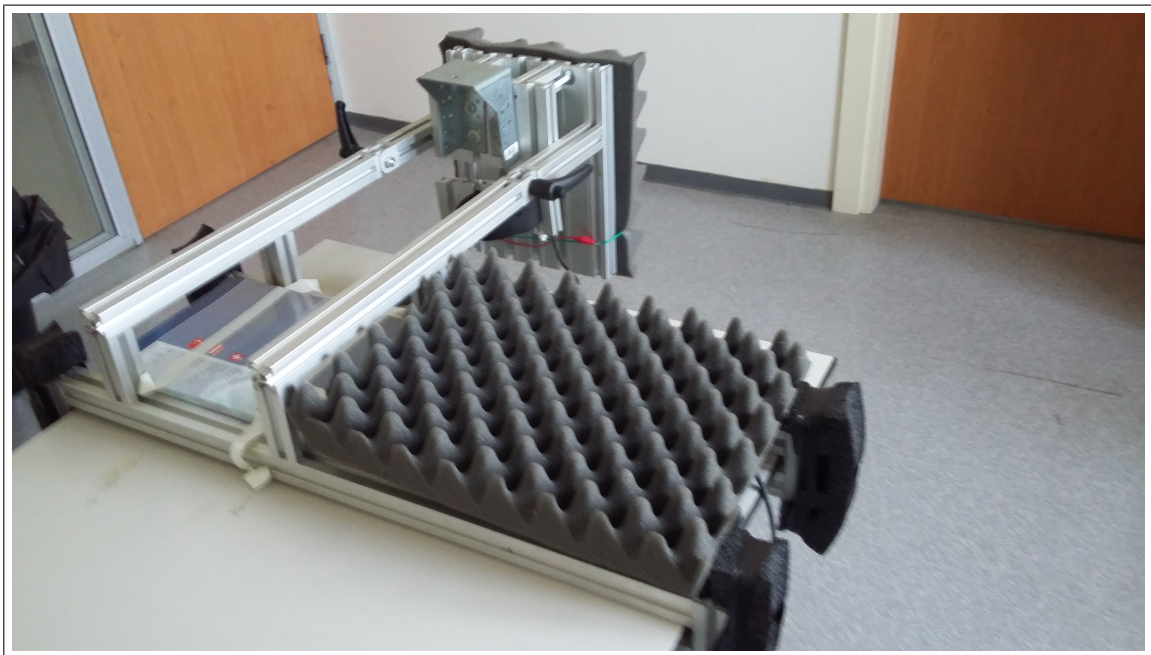
Figure 2.1 Custom-built MVIC measurement foot pedal.

Subjects were asked and verbally reinforced to perform MVIC during five seconds of plantar flexion followed by a two minutes of rest period. This was repeated three times and the highest plantar flexion force was determined to represent MVIC as long as the difference between subsequent measurements does not exceed 5%. If so, additional measurements were performed [53]. Subjects should be able to sustain 15% MVIC of the plantar flexion during MRI data acquisition. For that purpose, subjects

were trained to maintain force at 15% MVIC with the help of a visual feedback by
sustaining isometric plantar flexion during six minutes (Figure 2.2).
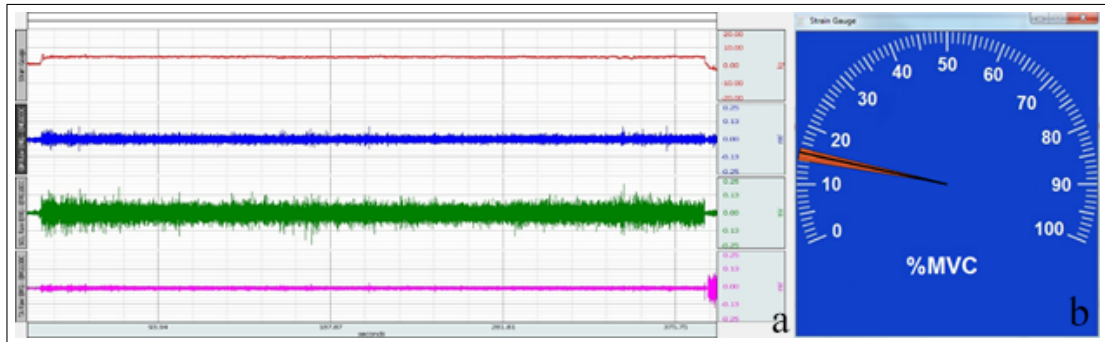
Figure 2.2 a) Force (red) and EMG (blue, green, pink from GM, SOL, TA correspondingly) signals
acquired during six minutes of 15% MVC of plantarflexion b) MVIC rate control interface

2.2.2 Data Acquisition

Subjects were positioned in a 3T clinical MR scanner (Siemens Magnetom Trio,
Erlangen, Germany) in foot first prone position. Right foot was firmly fixed to a strain
gauge embedded custom-built MRI compatible foot pedal at an ankle angle of 90°
using a piece of Velcro attached under the heel and strips over the ankle. The knee
was brought to fully extended position (mean±SD,175°±3°) and the immobility of this
joint was provided by a piece of Velcro attached over patella and also on the MRI table
(Figure 2.3). Care was taken not to exert additional loads to target muscle compart-
ments and tendons. Real time MVC rate control visual interface was transmitted to
an MRI compatible monitor (Telemed,Istanbul,Turkey) that allowed subjects to adjust
and maintain isometric plantar flexion force at target level. All data acquisitions were
performed in Kozyatağı Acıbadem Hastanesi, Istanbul. Note that both strain gauges
were calibrated using calibration weights prior to the experiments.

Two 6-channel surface coils were placed on both left and right side of the lower
leg for image acquisition (Figure 2.3). Anatomical data (MR images) were obtained in
a 3D turbo fast-low angle shot (3D Turbo FLASH) imaging sequence (Figure 2.4). The
region between the most proximal part of the head of the tibia and the most proximal
location of the transverse crural ligament was localized in the field of view (FOV).
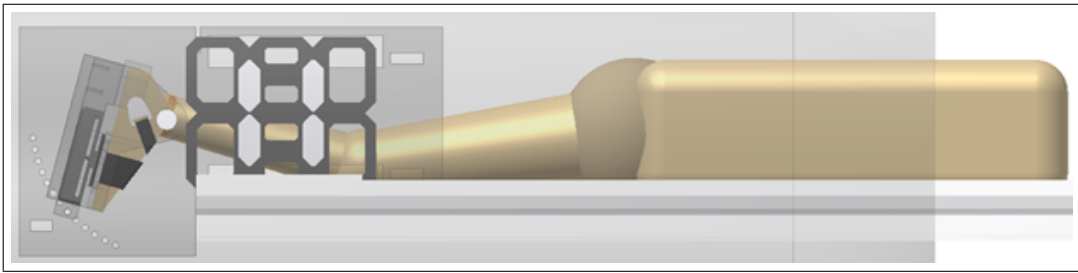
Figure 2.3 MRI compatible custom-built foot pedal and positioning of the subject (ankle angle equals 90° and knee is fully extended) in MR scanner.

Both left and right lower leg were imaged (Figure 2.6). In order to minimize potential chemical shifting artifacts, a high bandwidth was selected and frequency encoding was set at proximo-distal direction [54].
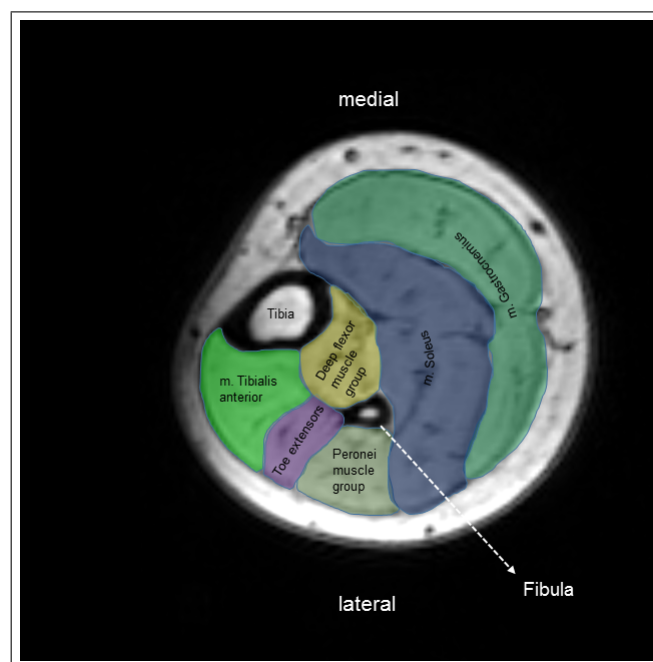
Figure 2.4 Muscles of the human lower leg segmented on the axial cross-section of the anatomical image.

Diffusion Tensor Imaging (DTI) was performed in the axial plane by using a single-shot echo planar imaging (ss-EPI) based multidirectional clinical DTI sequence. Proximal neck of the the tibia was selected as the starting point for FOV along longitudinal axis. Consequently, the region between this location and the end of the axial image stack (112 millimeters away from the beginning) constituted the FOV along longitudinal axis for DTI. Fat suppression and posterior-anterior direction frequency

encoding were applied so as to keep chemical shifting artifact away from region of interest (ROI). Only the right lower leg was imaged for DTI (Figure 2.6). Please see Table 2.2 for sequence parameters belonging to both MR and DT data acquisition. For

Table 2.2
MRI and DTI acquisition sequence parameters.

	MR imaging parameters	DT imaging parameters
Sequence Name	Turbo FLASH	ss-EPI
Slice Orientation	Coronal	Axial
Repetition Time (TR)(ms)	1750	4900
Echo Time (TE)(ms)	3.36	61
FOV (mm^2)	320X320	180X180
Reconstructed Matrix (mm^2)	320X320	l28X128
Pixel Size (mm^2)	1.0X1.0	1.4X1.4
Slice Thickness (mm)	1	2,8
Flip Angle (°)	12	90
Bandwidth (Hz/pixel)	130	2003
b-value (s/mm^2)	N/A	450
Number of Diffusion Gradients	N/A	12
Acquisition Time (mm:ss)	05:41	07:48

undeformed state image acquisition, subjects were asked to stay relaxed in abovementioned position (Figure 2.3). Next, maintaining the same position, subjects were asked to perform 15% MVIC of plantar flexion and to sustain the contraction at this level until the image acquisition is completed for deformed state image acquisition. MR and DT images were acquired for both deformed and undeformed state.

2.3   Post Processing

The aim is to quantify local deformations along the muscle fibers of GM. Such quantification requires a combination of information from two different image domains, (i) diffusion image domain for localizing deformed state GM tracts, (ii) anatomical image domain for voxel-wise strain tensor quantification. Finally, fiber direction strain

values are calculated by rotating strain tensors to the direction of the tracked muscle fibers (Figure 2.5).
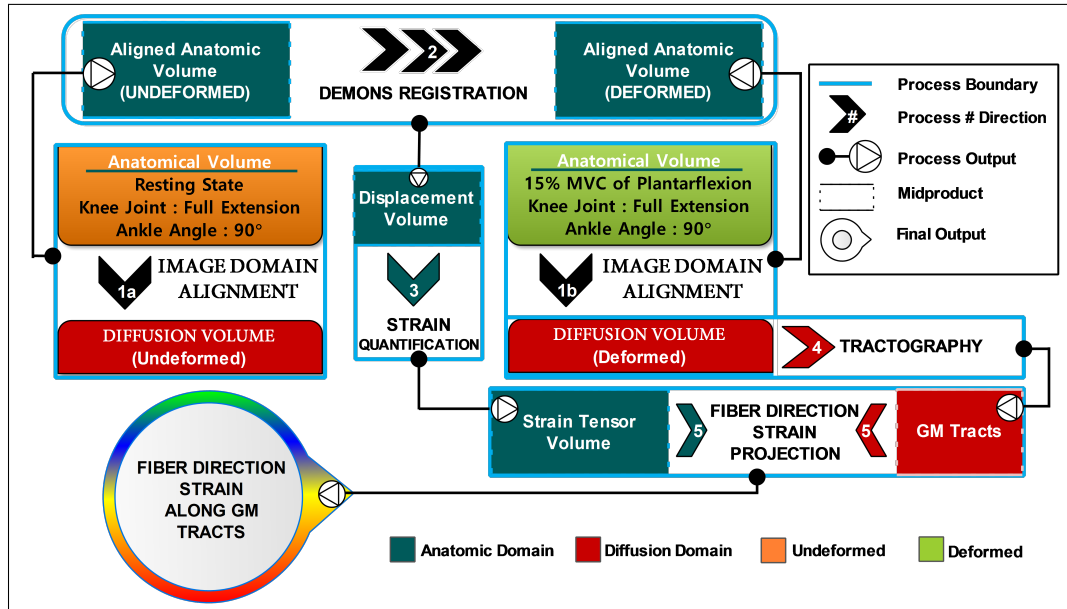
Figure 2.5 Image processing algorithmic flowchart.

2.3.1 Anatomical Image Domain Processes

2.3.1.1 Quantification of Displacement Volume

Demons algorithm is a deformable and non-parametric image registration algorithm based on the optical flow principles [44]. Demons algorithm takes two images as input and produces a displacement field, which represents the required transformation to match two images. Therefore, it solves the displacement vector for each voxel. For this purpose, it computes the image intensity gradient within the static image and relates it with the difference image of the static and moving image pixel-wisely by division. However, in the areas where image gradient is too small, flow becomes unstable and the displacement vector leads to an infinite value [55] In order to overcome this instability, Thirion's Demons algorithm regularizes the total displacement field at each iteration by smoothing it with a Gaussian kernel until convergence criterion is satisfied [56].

MR and DT images map on top of each other in the global coordinate system. Within the interval where both images overlap, they occupy the same volume with different resolutions and characteristics. Since subjects were not repositioned during experiment, DT and MR images were not registered prior to the Demons registration. However, MR images must be cropped properly in order to provide correct matching also in the image coordinates. Therefore, direction conventions of the MR images were matched with that of DT images. Next, MR images were cropped to match with their corresponding DT images in the image coordinates. In order to avoid boundary artifacts of Demons algorithm, MR images were cropped from 32mm above the superior and below the inferior boundary of the DT volume (Figure 2.6). Finally, undeformed MR volume was registered onto the deformed MR volume by implementing deformable Demons registration [57] in MATLAB R2012a (The Mathworks Inc.,Natick,MA).
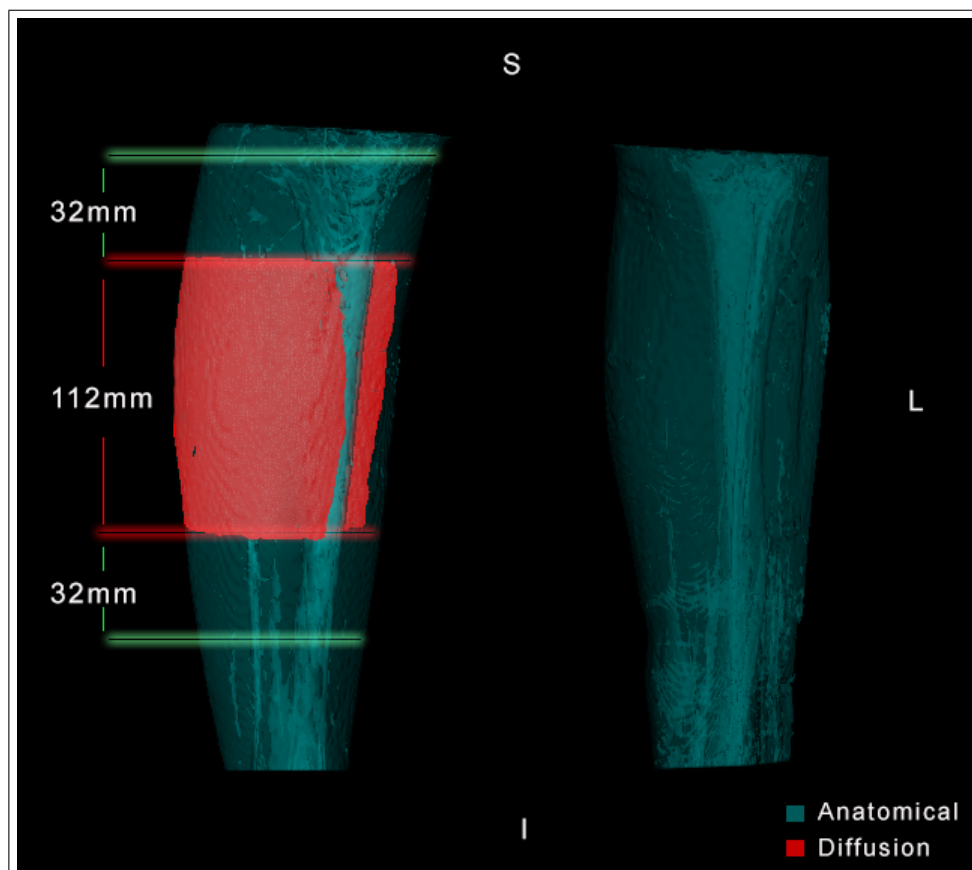
Figure 2.6 3D reconstructed whole MR (blue) and DT (red) volumes. The interval of 176mm between the green lines identifies the cropped volume to be registered with Demons

Displacement vectors obtained from Demons algorithm are described on the grid points of the undeformed (moving) image. However, deformed (fixed) state tracts are selected for strain projection. In order to provide appropriate matching between the deformed state GM tracts and quantified strain tensor field derived from the displacement field, displacement vectors on the grid points of the displacement field were transformed to their corresponding deformed state positions (Figure 2.7).
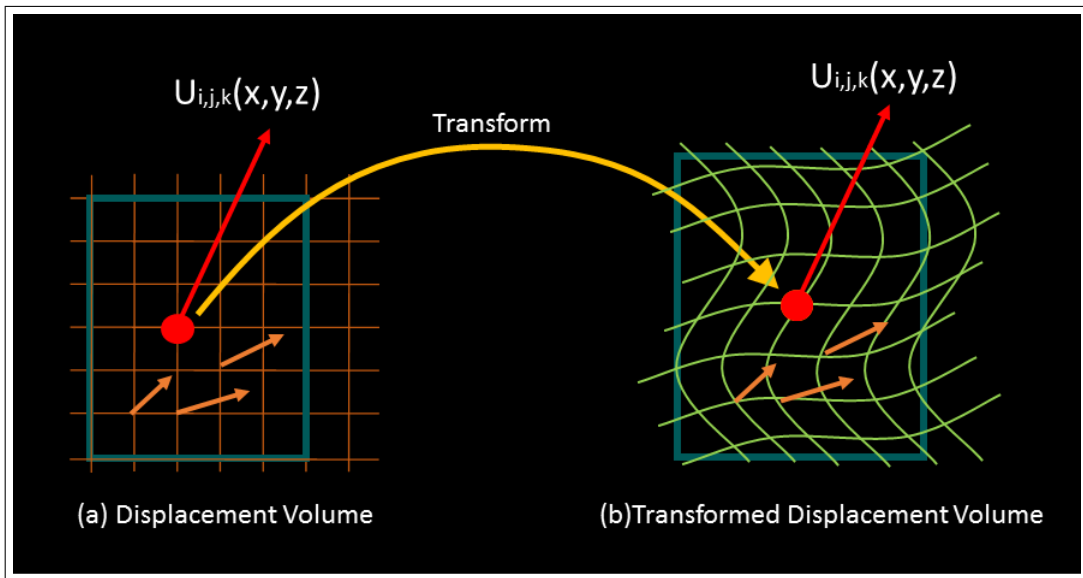
Figure 2.7 Transformation of the displacement volume to the deformed state

2.3.1.2 Quantification of Strain Tensor Volume

Each particle in a continuum body is characterized by a position vector for both undeformed (base) and deformed (current) configuration. Displacement of a particle with respect to a base configuration is defined by a displacement vector $\vec{u}$ that maps the base point $\mathbf{P}(\mathbf{X})$ to the current point $\mathbf{P}(\mathbf{x})$ (Figure 2.8). Therefore, displacement of all particles (i.e. voxels in this case) within a body constitutes a displacement field.

Deformation i.e., an alternation of the shape occurs if there is a relative displacement between the particles of the body, which is characterized by strain in continuum mechanics. Strains are expressed as a second order tensor ($\mathbf{E}$), which describes a

magnitude and two directions (normal and shear components) associated with it:

$$\mathbf{E} = \begin{pmatrix} e_{11} & e_{12} & e_{13} \\ e_{21} & e_{22} & e_{23} \\ e_{31} & e_{32} & e_{33} \end{pmatrix} \tag{2.1}$$
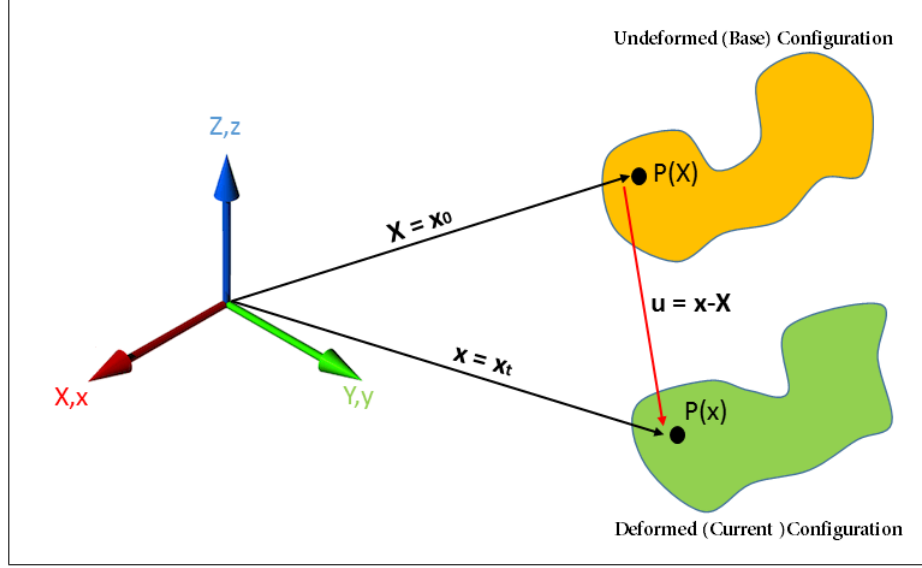
Figure 2.8 Geometric representation of undeformed and deformed configurations.

The displacement vector $\vec{u}$ in Lagrangian description expressed as:

$$\vec{u} = \begin{pmatrix} u_1 \\ u_2 \\ u_3 \end{pmatrix} = \begin{pmatrix} x - X \\ y - Y \\ z - Z \end{pmatrix} = x - X \tag{2.2}$$

The first step for quantify strain tensor field from a displacement field is arranging the derivatives of the position vectors of the undeformed (X, Y, Z) and the deformed (x, y, z) configurations in Jacobian format to obtain the *deformation gradient* $\mathbf{F}$:

$$\mathbf{F} = \frac{\partial(x,y,z)}{\partial(X,Y,Z)} = \begin{pmatrix} \dfrac{\partial x}{\partial X} & \dfrac{\partial x}{\partial Y} & \dfrac{\partial x}{\partial Z} \\ \dfrac{\partial y}{\partial X} & \dfrac{\partial y}{\partial Y} & \dfrac{\partial y}{\partial Z} \\ \dfrac{\partial z}{\partial X} & \dfrac{\partial z}{\partial Y} & \dfrac{\partial z}{\partial Z} \end{pmatrix} \tag{2.3}$$

Displacement gradients ∇u can be expressed with respect to both undeformed and deformed configurations. Displacement gradient with respect to the undeformed configuration is computed as follows:

$$\nabla u = \mathbf{F} - \mathbf{I} \tag{2.4}$$

where, I defines a 3×3 identity matrix. Finally, local deformations are quantified by calculating Green-Lagrange strain tensor, which is a suitable finite strain measure [58]:

$$\mathbf{E} = \frac{1}{2}(\mathbf{F}^T\mathbf{F} - \mathbf{I}) = \frac{1}{2}(\nabla u + \nabla u^T) + (\nabla u \nabla u^T) \tag{2.5}$$

2.3.2 Diffusion Image Domain Processes

Diffusion tensor tractography is an image processing application in which collected diffusion weighted images (DWI) are analyzed in order to visualize tracts belonging to certain structures within the FOV by making use of the anisotropic diffusion of the water molecules. Tractographic reconstruction provides information about *in-vivo* tissue characteristics and the 3D orientation of the reconstructed fibers; however, in macro-scale.

2.3.2.1 Diffusion Tensor Tractography for Medial Gastrocnemius Muscle

Denoising of the DWI volumes prior to the tensor estimation is critical [59]. Furthermore, application of the Rician statistics to the DWI has been shown to improve fiber orientation estimations [60]. On this basis, all gradient volumes were denoised using a joint-information Rician noise removal algorithm that uses the information given by all DWI channels, and the correlations between of them. Level estimation for the noise that follows a Rician distribution was performed using linear minimum mean square error estimator in MATLAB R2012a (The Mathworks Inc.,Natick,MA) [61]. Figure 2.9 shows the effect of noise removal on a single axial slice from a gradient volume. Following that, tensor estimation was performed for each voxel from denoised
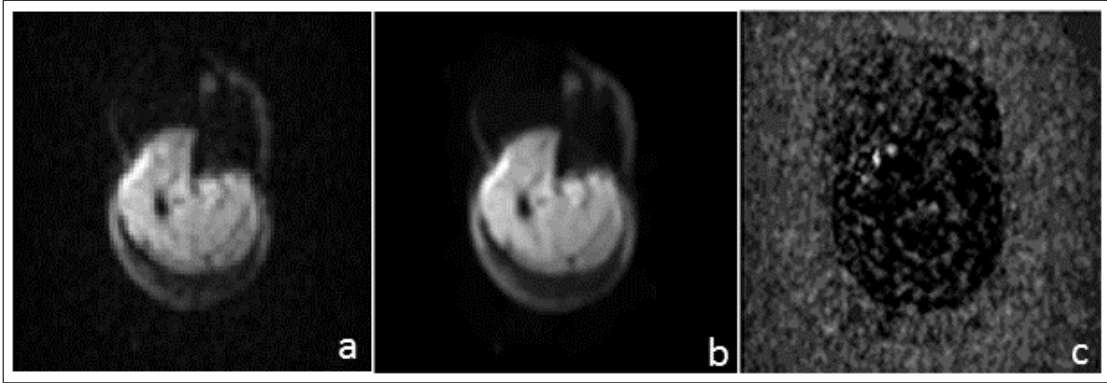
Figure 2.9 Effect of noise removal on DWI. a- Original image b- Denoised image c- Difference image

DWI. The tracts were reconstructed using a 4th order Runge-Kutta streamline integration algorithm [62] using a modified version of the $VAVframe^{TM}$ software (VAVlab, Istanbul, Turkey) [63, 64]. Log-Euclidean framework was used for diffusion tensor interpolation at non-integer grid points during tracking [65].

Set of termination conditions were defined based upon diffusion tensor and tract parameters so as to compute muscle tracts properly. Tract seed points were generated from voxels showing a minimum directionality of diffusion i.e., a fractional anisotropy (FA) of 0.1 [66]. The seed points were bi-directionally tracked with integration steps of 0.5 times the smallest voxel dimension [67] i.e., 0.7mm. Each of these integration points forms a fiber node. The tracts obtained were terminated based on diffusion tensor (DT) parameters including maximum FA of 0.5 and maximum curvature per integration step of 5° [66] and GM muscle geometry including minimum tract length of 30mm and maximum tract length of 50mm [68].

However, these parameters were not sufficient enough to segment GM tracts from their surroundings. To overcome this challenge, two polygonal region of interests (ROIs) were drawn around to GM on the axial b0 images of the deformed state DWI. Only the tracts passing both of these cross sectional ROIs were selected in the end of this preliminary segmentation. Next, further manual segmentation was performed to pick GM tracts solely. Locations of the anatomical boundaries of the GM and the orientations of the remained tracts were used in combination to select tracts that are

representing the *in-vivo* structure of the GM during 15% MVIC of sustained plantar flexion. This two-stage segmentation method yielded physiologically representative GM tracts that are convenient to be recruited for strain projection along of them (Figure 2.10c).
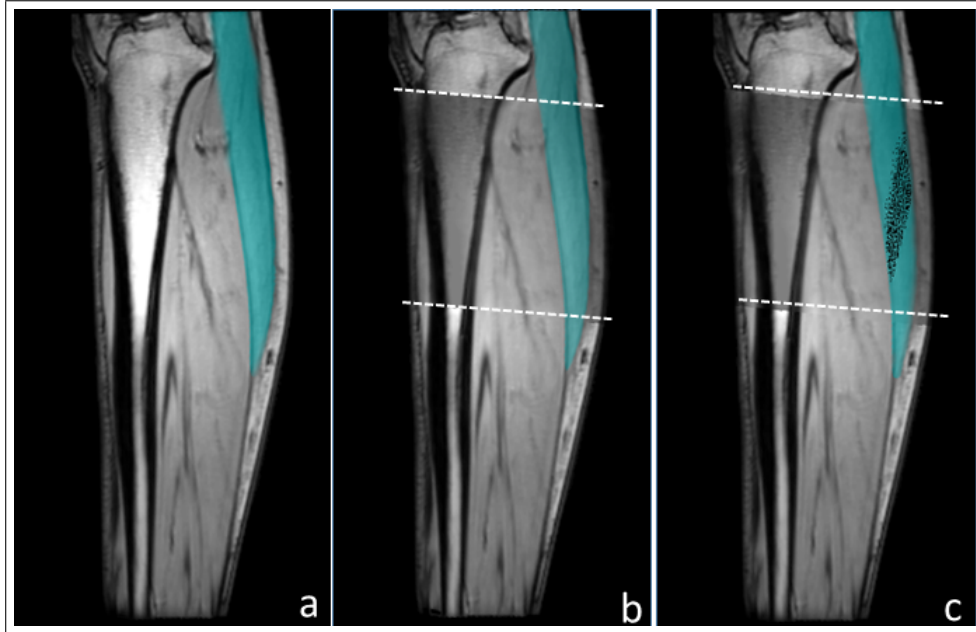
Figure 2.10 a- Representative MR image of human right lower leg during 15% MVC of isometric plantar flexion, showing a sagittal-oblique slice aligned with the longitudinal axis of the GM (blue). b- Sagittal-oblique DT image slice that matches with the superimposed portion of the MR image overlaid with 50% transparency between the white dashed lines. These lines indicate the superior and inferior limits of the DT image along longitudinal axis. c- Shows a profile view of the reconstructed GM tracts (black).

2.3.3 Combinational Processing of Diffusion and Anatomical Data

Quantification steps for strain tensor volume and GM tracts have been described so far. However, strain tensor volume expresses local deformations in terms of an outside coordinate system. From the point of physiological meaning of local deformations, it is critical to quantify strains in the direction of the muscle fibers. Hence, vector expression of the direction of the muscle fibers was given as a normalized tangent vector between two successive fiber tract nodes and denoted as $\vec{t}$ Next, strain coefficients (**SC**) were calculated from strain tensors (**E**) at each fiber node as follows [47]:

$$\mathbf{SC} = \vec{t}^T \mathbf{E} \vec{t} \tag{2.6}$$

Consequently, required information to compute directional component of the strain tensor was provided directly from deformed state GM tracts.

As the tractography step size between two fiber nodes is half of the smallest DT image voxel size, off-grid strain tensors must be interpolated to express a strain tensor on each fiber node. For this purpose, a linear interpolation was implemented within the neighborhood of 8 pixels:

$$\bar{\mathbf{E}} = \sum_{i=1}^{8} W_i E_i \tag{2.7}$$

where W_i represents normalized weights and E_i stands for the strain tensor at the ith neighbor, and ($\bar{\mathbf{E}}$) describes the interpolated strain tensor.

2.3.4   3D Visualization

A position vector in the global coordinate system and a corresponding strain coefficient were defined for each GM fiber node as a result of fiber direction strain projection along the GM tracts. Since MR images and DT images map on top of each other in the global coordinates, it is possible to visualize GM tracts in anatomical image domain. In order to implement such operation, GM tracts were firstly transferred into 3D Slicer [69]. Following manual segmentation of the tiba, fibula and GM on each axial slice of the MR images, volume construction was performed so as to visualize these structures three dimensionally. Finally, GM tracts were displayed at their corresponding locations within the translucently visualized 3D anatomical model of the GM. The tracts were colored according to scalar values (i.e., strain coefficients) using tractography display module of the 3D slicer software.

2.3.5   Estimation of Errors

The validity of Demons algorithm in quantifying tissue deformations was shown with effective testing [46]. Undeformed state MR images were transformed by a synthetic rigid body motion imposed on the data: 10° rotation within the cross-sectional plane (representing endorotation of the knee) [70], 3° rotation in the coronal and sagittal planes, and 4 mm translation axially. Subsequently, the undeformed state and these synthetically transformed image sets were compared. The displacement fields calculated using Demons algorithm were mapped onto the tracked fibers. Theoretically, imposed rigid body motion should cause no strains. Therefore, resulting strains calculated as described were used as estimates of error strains.

2.3.6   Statistics

Non-parametric Wilcoxon rank sum tests were performed to evaluate statistical significance of difference between experimental and error fiber direction strains for lengthening and shortening individually. The level of statistical significance was set at $p < 0.05$.

3. RESULTS

3.1 Statistical Significance of the Fiber Direction Strains

Pooled data over subjects show that mean error strains (1±1% for lengthening and 2±1% for shortening) are small and are statistically significantly different from mean fiber direction strains (13.7±12% for lengthening and 7.9±4% for shortening) occurring due to maintained plantar flexion activity at 15% of MVIC within the localized tracts of the GM (Figure 3.1a).
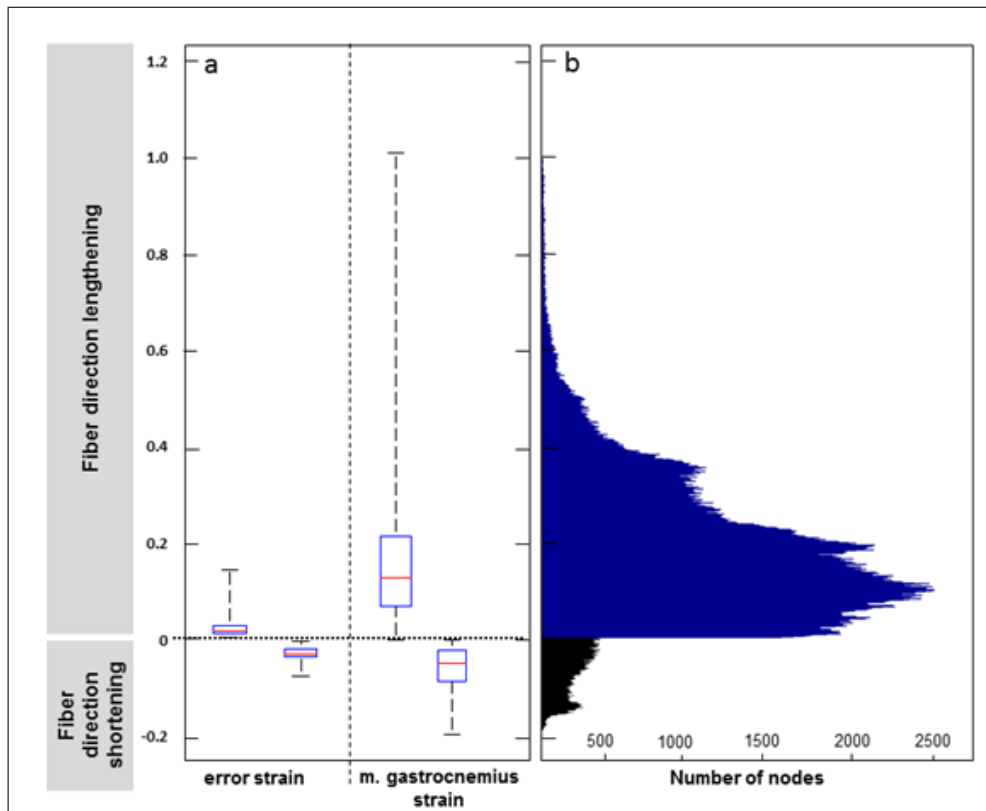
Figure 3.1 Pooled data over subjects shows the fiber direction local lengthening and shortenings occurred due to 15% MVIC of plantar flexion and the error strains within the localized tracts of the GM. a- Box and whisker plots : The horizontal line inside of the each box represents the median value; the upper and lower edges of the boxes represent upper and lower quartiles, respectively and lines extending from each end of the boxes (whiskers) indicate peak values of the fiber direction strain values calculated on each fiber node of GM for pooled data over subjects. b- Histogram of the pooled data over subjects represents the number of nodes with respect to the fiber direction lengthening (blue) and fiber direction shortenings (black) due to 15% MVIC of the plantar flexion within the localized tracts of the GM.

3.2 Serial Distribution of Strain along Muscle Fibers of Medial Gastrocnemius

Interquartile range (IQR) identifies the difference between upper and lower quartiles, which therefore can be considered as a measure of the heterogeneity of the strain distribution. Among all subjects, strain distribution is varied mostly for subject-B with an IQR of 31.0% i.e., lengthening and shortening together show the most heterogeneous distribution for this subject. The widest range in the fiber direction strain distribution (from 16.4% shortening to 108% lengthening) is also observed for the same subject. Whereas, subject-E shows the least heterogeneity for lengthening and shortening together, yet with a remarkable IQR of 8.7%. (Table 3.1).

Table 3.1
Statistical summary of fiber direction strain values for each subject and pooled data. (+) indicates
lengthening and (-) indicates shortening

Subject	A	B	C	D	E	Pooled
Maximum Lengthening	32.2%	108%	39.1%	57.4%	15.8%	108%
Maximum Shortening	17.8%	16.4%	13.3%	16.9%	21.3%	21.3%
Mean Lengthening	10.5%	22.7%	13.4%	1.6%	5.7%	13.7%
Mean Shortening	4.0%	7.7%	5.4%	4.9%	4.2%	5.2%
Mean	4.4%(+)	11.1%(+)	7.4%(+)	1.4%(+)	2.1%(+)	7.9%(+)
Median	2.3%(+)	5.2%(+)	6.0%(+)	13.8%(+)	2.3%(+)	5.2%(+)
IQR	14.5%	31.0%	17.9%	14.3%	8.7%	17.8%

Strain distribution shows a sizable heterogeneity in pooled data over subjects with an IQR value of 15.8% for lengthening and 7.0% for shortening. The maximum variation in the distribution of the fiber direction lengthening is observed for the subject-C with an IQR value of 14.2%, whereas fiber direction shortening varies mostly for subject-D with and IQR value of 5.7%. On the other hand, least heterogeneous fiber direction lengthening distribution is observed for subject-E with an IQR of 5.5% and least heterogeneous fiber direction shortening is observed for subject-B with an IQR of 2.7%. Nevertheless, these IQR values indicate a considerable heterogeneity for

the fiber direction local strain distributions.

Serial distribution identifies the representation of the fiber direction strain values within each muscle tract of GM, where each fiber node specifies a local fiber direction strain value. Figures 3.2 to 3.6 depict the serial distribution of the local strains occurred due to 15% MVIC of the sustained plantar flexion activity within the deformed state GM tracts. Independently of the characteristic of the strain pattern, all of these figures together suggest that lengthening and shortening (up to locally 108.0% and 21.4% for pooled data, respectively) and also simultaneously occur within the same GM tracts. For example, the maximum range of serial distribution along an individual tract (remained almost constant at the origin and lengthened 108.0% locally at the insertion of a 38.5 millimeters long tract) is observed for subject-B among all subjects as can be seen from Table 3.2. In addition all of the single tracts represented in this table show the minimum local strain in the origin, whereas they show the maximum local strain in the insertion along their orientations.

Table 3.2
Peak strain values and the length of the single tract that has the widest range of strain distribution among all tracts within that subject. (+) indicates lengthening, (-) indicates shortening and (0) stands for constant length.

Subject	Local maximum	Local minimum	Length of the tract (mm)
A	32.2% (+)	11.5% (-)	36.4
B	108.0% (+)	0.0% (0)	38.5
C	36.7% (+)	12.4% (-)	46.9
D	52.1% (+)	16.3% (-)	46.8
E	13.4% (+)	5.2% (-)	33.6

In the majority of the results (Figures 3.2 to 3.6), serial distribution seems to indicate that local strains closer to the superficial aponeurosis (towards origin, more proximal) of GM tend to indicate shortening, whereas local strains closer to the deep aponeurosis (towards insertion, more distal) are more likely to indicate lengthening generally. However, serial distribution reveals a more complex characteristic especially for subject-E (Figure 3.6).

3.3 Parallel Distribution of Strain between Muscle Fibers of Medial Gastrocnemius

Parallel distribution is the representation of the mean fiber direction strains for each tract i.e., each fiber node represents the mean fiber direction strain belonging to that tract. A representative result for parallel distribution is shown for subject-C (Figure 3.7) reveals that mean fiber direction strain occurs non-uniformly throughout the GM tracts. It can also be seen that shortening and lengthening occurs together in parallel distribution.

Consequently, 15% MVIC of the sustained plantar flexion activity with an ankle angle of 90° and fully extended knee configuration results in a serial distribution along the orientation of the muscle fibers of GM and confirms our hypothesis.

Figure 3.2 Three dimensional visualization of the deformed GM tracts of Subject-A. Tracts are colored with respect to the serial distribution of the strain due to 15% MVIC of the plantar flexion and placed on their corresponding positions within the deformed state MR image domain. Tibia and fibula (pale-gold) are visualized three dimensionally to convey orientation of the lower leg. GM (tile red,half translucent) is also rendered for conveying the three dimensonal sense of the tract orientation with respect to the GM anatomy. Colorbar presents the range of local fiber direction strains occured within the visualized tracts. Positive strain indicates lengthening and negative strain indicates shortening.
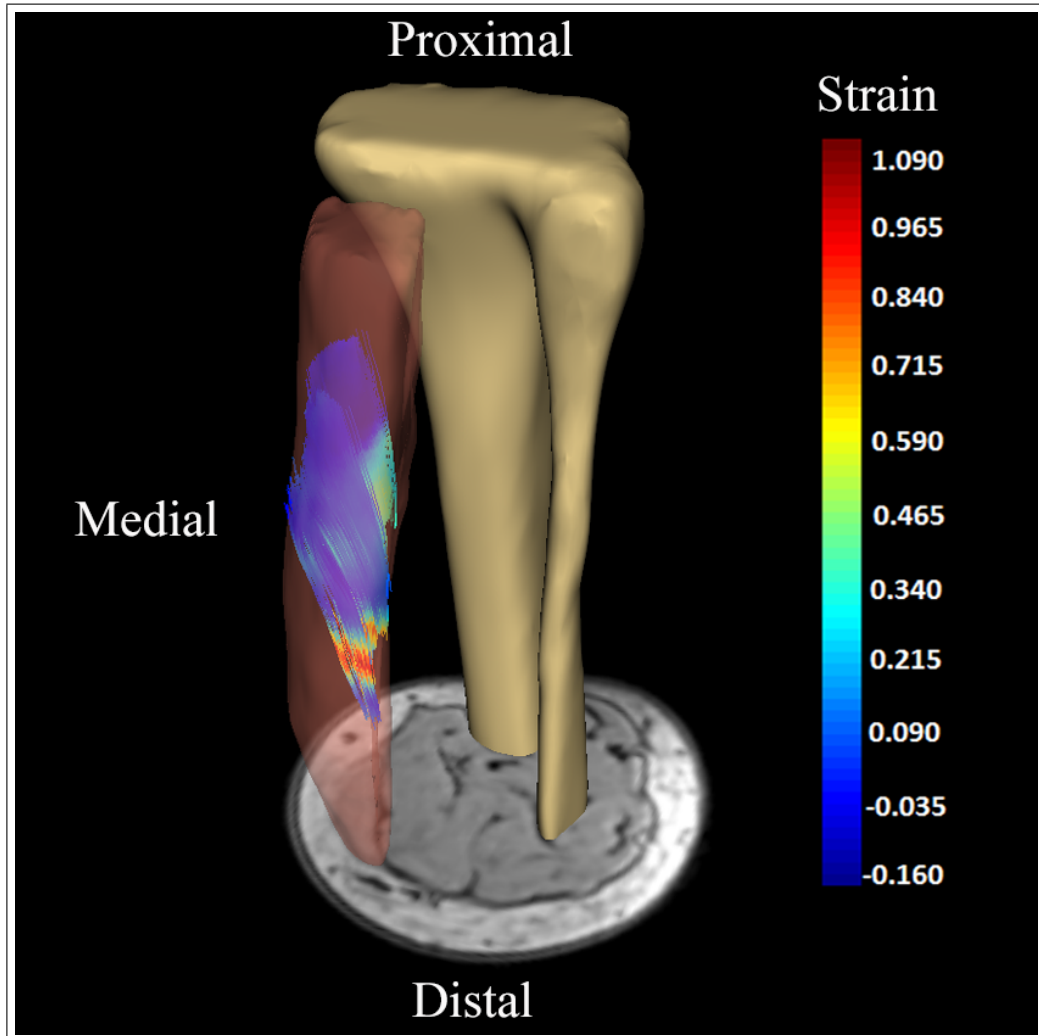
Figure 3.3 Three dimensional visualization of the deformed GM tracts of Subject-B. Tracts are colored with respect to the serial distribution of the strain due to 15% MVIC of the plantar flexion and placed on their corresponding positions within the deformed state MR image domain. Tibia and fibula (pale-gold) are visualized three dimensionally to convey orientation of the lower leg. GM (tile red,half translucent) is also rendered for conveying the three dimensonal sense of the tract orientation with respect to the GM anatomy. Colorbar presents the range of local fiber direction strains occured within the visualized tracts. Positive strain indicates lengthening and negative strain indicates shortening.
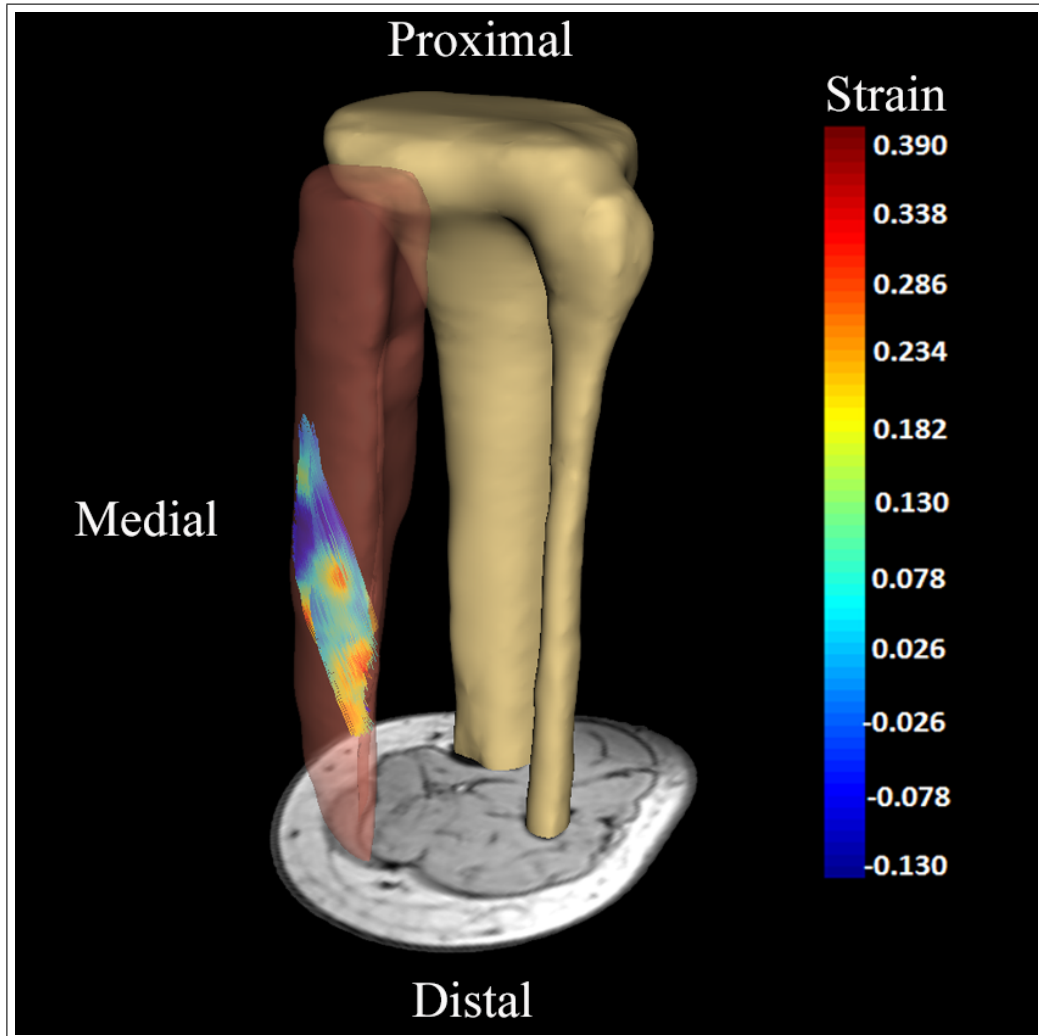
Figure 3.4 Three dimensional visualization of the deformed GM tracts of Subject-C. Tracts are colored with respect to the serial distribution of the strain due to 15% MVIC of the plantar flexion and placed on their corresponding positions within the deformed state MR image domain. Tibia and fibula (pale-gold) are visualized three dimensionally to convey orientation of the lower leg. GM (tile red,half translucent) is also rendered for conveying the three dimensonal sense of the tract orientation with respect to the GM anatomy. Colorbar presents the range of local fiber direction strains occured within the visualized tracts. Positive strain indicates lengthening and negative strain indicates shortening.

Figure 3.5 Three dimensional visualization of the deformed GM tracts of Subject-D. Tracts are colored with respect to the serial distribution of the strain due to 15% MVIC of the plantar flexion and placed on their corresponding positions within the deformed state MR image domain. Tibia and fibula (pale-gold) are visualized three dimensionally to convey orientation of the lower leg. GM (tile red,half translucent) is also rendered for conveying the three dimensonal sense of the tract orientation with respect to the GM anatomy. Colorbar presents the range of local fiber direction strains occured within the visualized tracts. Positive strain indicates lengthening and negative strain indicates shortening.
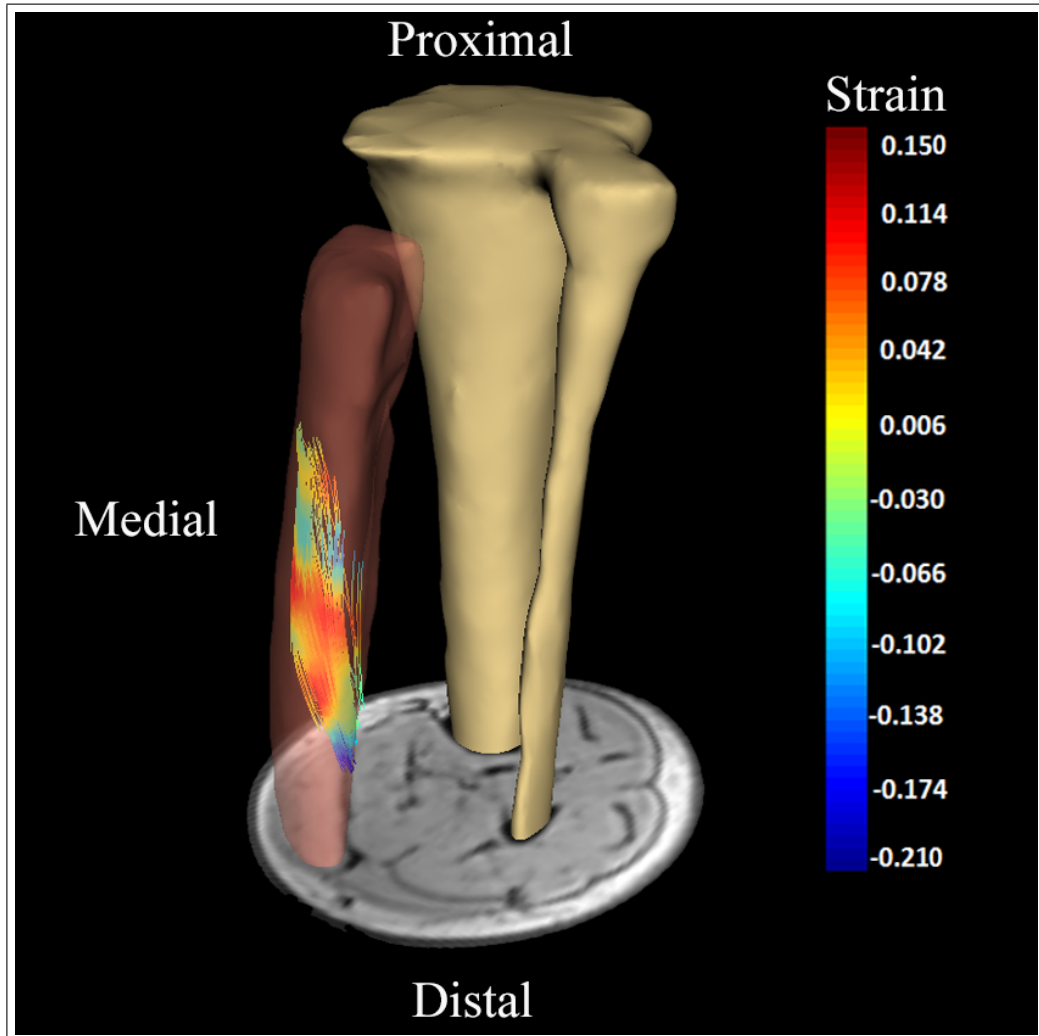
Figure 3.6 Three dimensional visualization of the deformed GM tracts of Subject-E. Tracts are colored with respect to the serial distribution of the strain due to 15% MVIC of the plantar flexion and placed on their corresponding positions within the deformed state MR image domain. Tibia and fibula (pale-gold) are visualized three dimensionally to convey orientation of the lower leg. GM (tile red,half translucent) is also rendered for conveying the three dimensonal sense of the tract orientation with respect to the GM anatomy. Colorbar presents the range of local fiber direction strains occured within the visualized tracts. Positive strain indicates lengthening and negative strain indicates shortening.
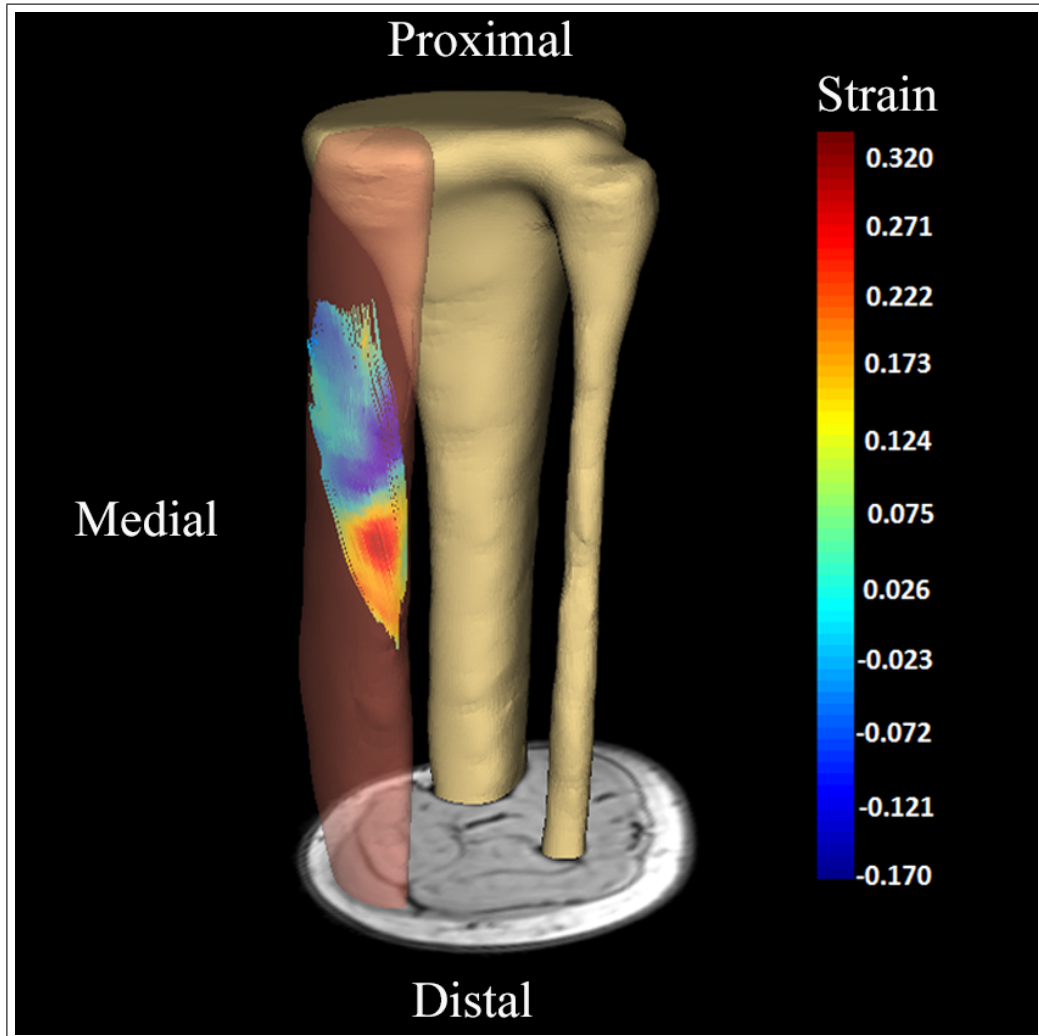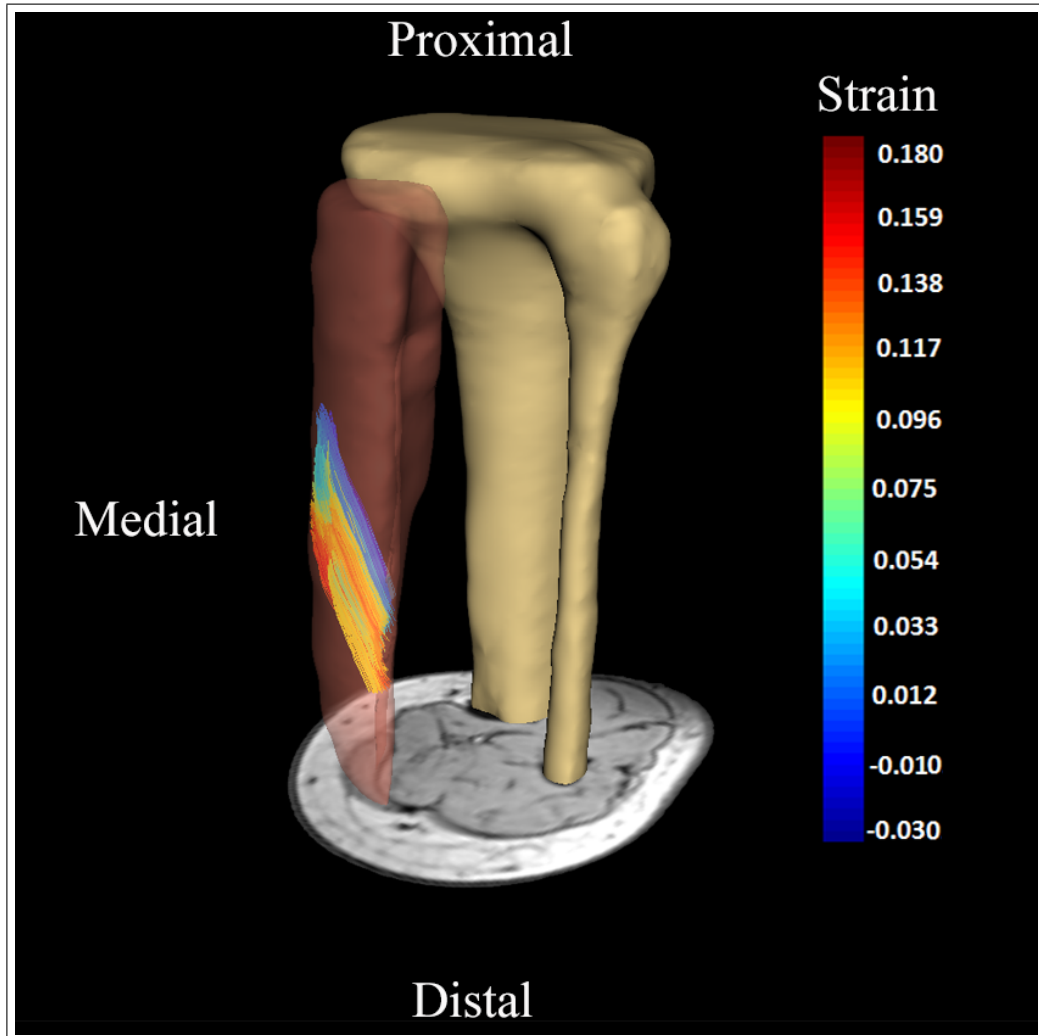
Figure 3.7 Three dimensional visualization of the deformed GM tracts of Subject-C. Tracts are colored with respect to the parallel distribution of the strain due to 15% MVIC of the plantar flexion and placed on their corresponding positions within the deformed state MR image domain. Tibia and fibula (pale-gold) are visualized three dimensionally to convey orientation of the lower leg. GM (tile red,half translucent) is also rendered for conveying the three dimensonal sense of the tract orientation with respect to the GM anatomy. Colorbar presents the range mean fiber direction strains occured within the visualized tracts. Positive strain indicates lengthening and negative strain indicates shortening.
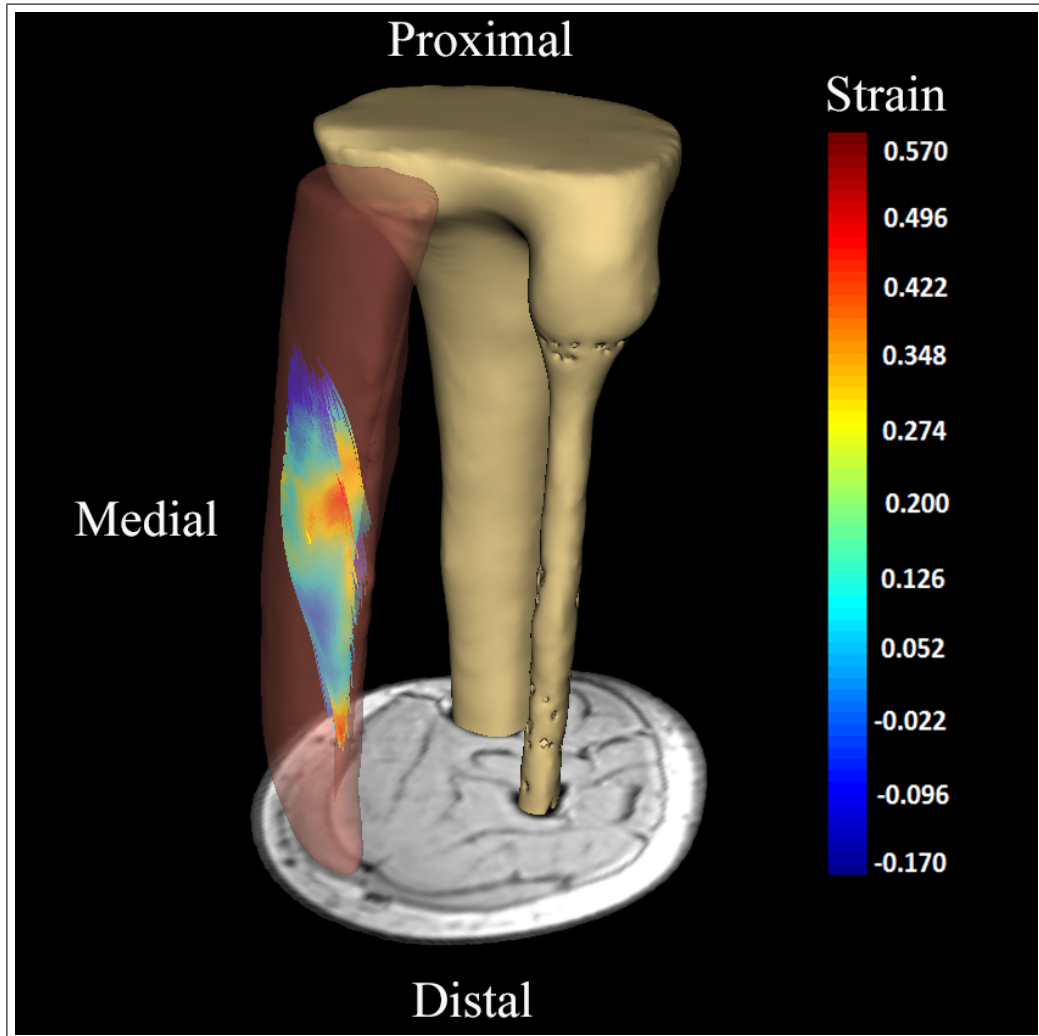
4. DISCUSSION

In this study, we have provided a demonstrative 3D representation of *in-vivo* local deformations with reference to the representative GM fiber tracts. 15% MVIC of sustained plantar flexion was studied by combining MRI, DTI, non-rigid image registration and advanced image processing methods. Our findings show a considerable heterogeneity, which occurred in both magnitude and the characteristics, for the serial strain distribution along the reconstructed muscle fiber tract orientations for each subject. Moreover, parallel distribution (i.e., tract-wise mean strain distribution in cross-fiber direction) also occurs non-uniformly among reconstructed GM tracts of each subject. This is particularly important because, such effects have a key role in the characterization of the mechanical functions of the skeletal muscles. Notably, this is the first study to our knowledge to investigate *in-vivo* myofascial force transmission effects with regards to the quantified length changes in the direction of GM fibers in active condition.

4.1 Representability of the Reconstructed Tracts

Several MRI studies from the literature have referred to the importance of strain representation along muscle fibers [27, 28, 38, 45]. Fundamental importance of such representation stems from the fact that sarcomeres are arranged in series within the myofibers. Therefore, evaluating length changes along this direction yields physiologically relevant information. It also has a further meaning from the perspective of myofascial force transmission, because muscle fibers are linked to the extracellular matrix along their full length. If these links are able to transmit force, sarcomere lengths may not be homogeneous and strain along muscle fiber tracts can quantify that. Proper localization of the skeletal muscle tracts therefore has a key importance.

Similar local fiber orientations and the leaning of the reconstructed muscle tracts

to run from origin to insertion at length are the expected patterns for a convenient muscle fiber geometry [21]. As evident in Figure 3.7, reconstructed GM tracts compare well with these conditions. Furthermore, they show a demonstrative consistency with the GM anatomy. GM is a unipennate muscle with spanning fibers [71]. Its fibers originate from the superficial aponeurosis at the dorsal aspect of the muscle, run along the anteroinferior direction, and attach to the deep aponeurosis at the ventral aspect over whole muscle length [72]. Such structural orientation is saliently visible in Figures 3.2 to 3.6.

Analysis of muscle strain due to isometric activation with respect to muscle fiber direction using dynamic MRI methods have limited applicability because such imaging sequences require highly repetitive and consistent movements to encode tissue motion correctly [14, 17, 18]. On the other hand, DTI acquisition is adversely affected by the motion of the target within the FOV, which in turn requires images to be acquired while target is stationary. As a result, these restrictions together oblige strain values, acquired from multiple time frames, to be related with fiber directions from a certain time frame. Furthermore, these operations must be performed on a single slice in a certain 2D image plane. At this point, strain quantification using Demons algorithm has its advantage over dynamic imaging methods, because it enables the computation of the displacements between two separate image sets, and in 3D image coordinates. Since these images are acquired while the target it stationary, fiber directions representing each state can be obtained using DTI and strains can be represented with reference to the corresponding muscle fiber orientations.

In sum, successfully applied experimental techniques in this study have enabled representation of strains in 3D with reference to the orientation of muscle fibers. The data are representative for both tested functional state (15% MVIC of sustained plantar flexion) and the anatomical structure of GM fibers.

4.2 Serial Distribution of the Strain

From the perspective of classical approach on skeletal muscle mechanics, force transmission is considered to take place solely at the myotendinous junctions [33]. Such presumption implicitly implies that extracellular matrix and muscle fibers are mechanically connected only at the fiber ends. Under this assumption, length changes along the direction of the skeletal muscle fibers are considered to be distributed uniformly. In contrast, it is evident from the present results (Figures 3.2 to 3.6) that 15% MVIC of sustained plantar flexion results in heterogeneous serial distribution along muscle fibers.

An activated sarcomere shortens to its active slack length unless the force it generates counteracted by an external force [73]. Hence, shortening along the GM muscle fiber direction is plausible due to 15% MVIC of plantar flexion. However, our results indicate that both positive and negative strains are found together within the same fiber tracts. Presence of such heterogeneous serial distribution within the individual tracts therefore points out that there are additional force transmission pathways other than myotendinous junctions.

Each skeletal muscle cell has a cytoskeletal protective network against mechanical stress that surrounds myofibrils at the z-discs by a special filament termed as desmin. Desmin inserts into sarcolemma at the regions known as costameres. These costameres are responsible for transducing contractile force from the z-disk to basal lamina and plays an important role in stabilizing the myofibril positions and maintaining structural integrity of the sarcolemma [74]. Such example of an integrated intracellular organization highlights the mechano-functional importance of the force transmitting abilities of the sarcolemmal structures. Furthermore, connections provided by the trans-sarcolemmal molecules between cytoskeleton and laminin eventually provides a connection between extracellular matrix and muscle fiber domain. Because, laminin is linked to basal lamina, which envelops the sarcolemma and is mechanically attached to the endomysium. It has been shown that these connections are able to lateral transmission of the force between endomysium and muscle fibers [36].

Presence of such additional force transmission pathways other than myotendinous junctions, continuity of the extracellular matrix at the each level of organization (i.e., from endomysium to the superficial fascia) and the connections between intramuscular and extramuscular tissues (e.g., neurovascular tracts) lends support to the heterogeneous length changes along the direction of the muscle fibers that we have observed in this present study. These findings are in good agreement with finite element modeling studies [4, 42, 43] and implies the *in-vivo* occurrence of the myofascial force transmission effects on the sarcomere length changes during muscle activation. Such heterogeneity has considerable effects on muscle length-force and force generation characteristics [37, 73]. Moreover, muscle length range of force exertion has been shown to be enhanced by serial sarcomere length distribution [75].

It has been shown that muscle relative position change is a major co-determinant of the muscle force [12]. Taking the joint configurations (Figure 2.3) into consideration, it is reasonable to assume that relative position of the GM with respect to its synergist SOL might be changed on account of the imposed knee extension. This is possible mainly because of the strategic adjacency of the SOL and the GM. The GM is a bi-articular muscle that spans both knee and ankle joints, whereas the SOL is a mono-articular muscle and spans the ankle only. Therefore, the SOL is under a globally isometric condition with respect to the any change in knee configuration. Moreover, it is known from the literature that a poly-articular muscle is expected to show more pronounced length changes relative to its mono-articular neighbor and therefore a substantial change in its relative position [73]. Although contribution of such position change to the deformation was not involved in Demons image registration, it could had pronounced the effects of myofascial force transmission. Because, proximally lengthening of the GM due to full knee extension may result in stretching inter- and extramuscular connections between these two muscles. Consequently, it is reasonable to consider the contribution of muscle relative position change to noticeable strains and heterogeneity occurred in the GM on account of the low-level isometric plantar flexion.

4.3   Parallel Distribution of the Strain

Our findings indicate that 15% of MVIC of sustained plantar flexion results not only in a serial distribution along the muscle fiber direction, but also in a heterogeneous parallel distribution between the muscle tracts of the GM (Figure 3.7). Appreciably, this is in concert with our expectations considering that such serial distribution has occurred within the GM tracts upon an isometric contraction. Results from a previous finite element study have reported that parallel distribution is found particularly at higher muscle lengths and the presence of such distribution indicates the effect of the intermuscular interactions [39] and shown to result in an enhanced range of muscle length [76].

Force modulation of a skeletal muscle is controlled by recruitment of more or fewer motor units and the rate coding of individual motor units [77]. It is known from the literature that low-level prolonged isometric contractions show time dependent recruitment characteristics. Fallentin et al. [78] observed that during long lasting isometric elbow flexion at 10% MVC (up to 2 hours) the number of recruited motor units increases with respect to time. Due to relatively short sustaining time and the 15% MVIC plantar flexion, it is plausible that only a subset of the GM motor units were recruited presently. In other words, some of the muscle fibers were not activated. In a previous finite modeling study, which is tailored for investigating of the effects of botulinum toxin, it has been reported that mean fiber direction strain values for the paralyzed muscle fibers show limited shortening or even lengthening depending on the location of the paralyzed muscle fibers [79]. Such effect termed as longer sarcomere effect applies also to the activated muscle fibers of partially paralyzed muscle and is attributed to the muscle fiber and the extracellular matrix interactions. This in turn resulted in a heterogeneous mean fiber direction strain distribution. These findings therefore may lend a support for the explanation of the lengthened tracts within the parallel distribution. However, it should be noted that due to restrictions posed by MRI, it was not possible to record electromyography (EMG) activities during the sustained contraction. Motor unit recruitments and rate coding measurements were not performed prior to the scan. Future study work should focus on motor unit recruit-

ment and rate coding characteristics of the GM during 15% MVIC of sustained plantar flexion during the experimentally employed acquisition time, outside of the scanner.

4.4 Implications of the Study

Intraoperative experiments during muscle lengthening surgery have highlighted the clinical importance of myofascial loads for spastic muscles [51,80,81]. In addition, *in-situ* animal experiments [82,83] and finite modeling studies [79,84] have investigated the effect of botulinum toxin administration, which is commonly used for treating spastic muscle. Although the authors did not explicitly refer to the effects of myofascial loads, the results of an *in-vivo* MRI study in which remedial surgery effects were investigated [18]. This implies the importance of inter- and extramuscular connections to mechanical functioning of skeletal muscles. These authors showed indicating mechanical interaction between the target muscles. It is obvious that *in-vivo* assessment of post operational effects of remedial surgery has a key importance. Furthermore, *in-vivo* effects of botulinum toxin administration remain unknown. The experimental techniques applied and improved within this study have potential uses for such *in-vivo* investigation of clinical applications and the effects of myofascial interactions on them. Further, these techniques enable the simultaneous evaluations of the fiber direction strain distribution within synergistic and antagonistic muscles, however further work is needed for improving of DTI acquisition techniques to be able to obtain artifact free image regions also, for the frontal muscle compartments e.g., tibialis anterior.

Since the GM is demanded for rapid actions like jumping or running, it is one of the most common sites for injury and tears [85]. For example isolated GM tear, which is also known as tennis leg syndrome, is commonly encountered [86]. Therefore, evaluation of *in-vivo* strain distribution characteristics in the direction of healthy GM tracts may contribute to the understanding of such pathologies, which in turn highlights the importance of the potential use of this method in sports science.

4.5   Limitations of the Study

DTI provides information about the structural properties of microstructures, however it uses a macroscopic technique (fascicle level) to visualize these structural properties. Although DTI enables evaluation of the strain distribution in the direction of the muscle fibers, these length changes do not explicitly imply sarcomere length changes due to limited resolution.

In order to decrease acquisiton time, DTI images were acquired from a certain region of the lower leg. As a result, feasibility of fiber direction strain quantification is limited by the FOV of DTI acquisition (Figure 2.10b). In addition, fiber segmentation methods that we have applied in order to obtain physiologically representative GM tracts resulted in the restriction of the fibers within a certain volume along the proximo-distal direction. Nevertheless, the number of reconstructed tracts both along the longitudinal and transverse directions was shown to be sufficient to represent the structure of the GM (Figure 2.10c).

MRI and DTI acquisitions require subjects to maintain isometric plantar flexion during the whole acquisition time. However, the subjects did not show a considerable sign of fatigue during image acquisition for 15% MVIC of sustained plantar flexion. Activation level is bound to the limitation that is posed by the long image acquisition time.

4.6   Prospective Studies

For a better understanding of the intermuscular effects, skeletal muscles should be evaluated together with their synergistic or even antagonistic counterparts. Therefore, an important question for the future studies is to investigate length change characteristics along the muscle fiber of the SOL along with the GM. Moreover, it is also feasible to determine muscle relative position change between the SOL and the GM,

which is within the bounds of possibility due to isometric plantarflexion. It has been previously reported that all voxels within the GM moved proximally [14] owing to 20% MVIC of plantarflexion, however information for the SOL was not provided. Consequently, calculation of global length changes of GM and SOL, and the interpretation of the magnitude and direction of displacement vectors obtained from Demons algorithm would provide an efficient method to evaluate muscle relative positon changes. Such position changes were shown to be the key determinants of myofascial force transmission effects [37, 41]

Despite the fact that maximum level of contraction is restricted by the relatively long scan time, lower level of contractions e.g., 5% MVIC can be studied. Within-subject comparison of the serial and parallel distributions of 5% MVIC and 15% MVIC of plantar flexion activities may provide a further insight to explain these exciting results represented by this study. Moreover, the next stage should involve the assessment of fiber direction length changes due to sustained isometric contractions with respect to the knee angle alterations.

Muscle fiber tracts, which represent the GM fascicles, have been reconstructed with a high angular resolution. Therefore, changes in the pennation angles of the GM tracts upon contraction is also within the bounds of the possibility. However, it should be noted that fiber direction strain values have been quantified with respect to the deformed state (15% MVIC of plantar flexion) tracts. For such comparison, undeformed state tractography must be performed also.

It would also be beneficial to evaluate the elongation of the reconstructed tracts between the origin and the insertion points to clarify that the tracts represent non-tendinous components, solely. As myofibres approach their tendinous origin or insertion, their diameter decreases substantially and the sarcolemma folds extensively in the myofibers longitudinal direction [32]. Depending on the fact that diffusion of the water molecules is restricted by the organizational arrangements, diffusion anisotropy indices (e.g., FA) may therefore be affected by virtue of such structural changes near the tendinous terminations. Assessment of the changes in FA values within tracked GM muscle

fibers with respect to their distance to the superficial and deep aponeuroses should therefore be a starting point to describe the elongation of the reconstructed tracts.

5. CONCLUSION

Improvement and successful application of the experimental techniques based on MRI have enabled the quantification of *in-vivo* local deformations along the fiber direction of the human medial gastrocnemius that undergoes submaximal isometric activation. To our knowledge, this is the first study in the literature that enables the assessment of such physiologically relevant information. Results from five healthy female subjects have shown that strain distribution within individual fibers and mean length changes in different fibers show a remarkable heterogeneity. These findings point out the presence of force transmission in the cross-fiber direction, which is termed as myofascial force transmission . Therefore, the classical point of view on skeletal muscle mechanics which considers that force transmission takes place solely in the myotendinous junctions is not tenable. Because, such consideration implies that skeletal muscles are independent actuators and they undergo uniform length changes upon any activation. Since it has physiological influences on the muscle length range of force exertion, heterogeneous length change in the muscle fiber direction is clinically relevant. Therefore, investigation of such distribution characteristics has a key importance in the etiology of spastic paralysis and also provides a better understanding of the mechanical interactions between skeletal muscles within their surroundings. Furthermore, present experimental methods form a basis for future studies to be focused on the *in-vivo* effects of botulinum toxin treatment on the mechanical behavior of skeletal muscle.

REFERENCES

1. Huxley, H., and J. Hanson, "Changes in the cross-striations of muscle during contraction and stretch and their structural interpretation," *Nature*, Vol. 173, pp. 973–976, 1954.

2. *Anatomy diagram of skeletal muscle.* Available: http://anatomyarea.com/neck-anatomy-diagram-3, Accessed on May 2015.

3. Kandel, E., J. Schwartz, T. Jessell, S. Siegelbaum, and A. Hudspeth, *Principles of Neural Science, 5th ed.*, McGraw-Hill, 2013.

4. Yucesoy, C., B. Koopman, G. Baan, H. Grootenboer, and P. Huijing, "Effects of inter- and extramuscular myofascial force transmission on adjacent synergistic muscles: Assessment by experiments and finite-element modeling," *J Biomech*, Vol. 36, pp. 1797–1811, 2003.

5. Ito, L., Y. Kawakami, Y. Ichinose, S. Fukashiro, and T. Fukunaga, "Nonisometric behavior of fascicles during isometric contractions of a human muscle," *Journal of Applied Physiology*, Vol. 85, pp. 1230–1235, 1998.

6. Kawakami, Y., Y. Ichinose, and T. Fukunaga, "Architectural and functional features of human triceps surae muscles during contraction," *Journal of Applied Physiology*, Vol. 85, pp. 398–404, 1998.

7. Lichtwark, G., K. Bougoulias, and A. Wilson, "Muscle fascicle and series elastic element length changes along the length of the human gastrocnemius during walking and running," *Journal of Biomechanics*, Vol. 40, pp. 157–164, 2007.

8. Ishikawa, M., P. Komi, M. Grey, V. Lepola, and G. Bruggemann, "Muscle-tendon interaction and elastic energy usage in human walking," *J Appl Physiol*, Vol. 99, pp. 603–608, 2005.

9. Ishikawa, M., J. Pakaslahti, and P. Komi, "Medial gastrocnemius muscle behavior during human running and walking," *Gait Posture*, Vol. 25, pp. 380–384, 2007.

10. Kwah, L., R. Pinto, J. Diong, and R. Herbert, "Reliability and validity of ultrasound measurements of muscle fascicle length and pennation in humans: A systematic review," *J Appl Physiol*, Vol. 114, pp. 761–769, 2013.

11. Rana, M., G. Hamarneh, and J. Wakeling, "3d fascicle orientations in triceps surae," *J Appl Physiol*, Vol. 115, pp. 116–125, 2013.

12. Yucesoy, C., "Epimuscular myofascial force transmission implies novel principles for muscular mechanics," *Exercise and Sport Sciences Reviews*, Vol. 38, pp. 128–134, 2010.

13. Reeves, N., and M. Narici, "Behavior of human muscle fascicles during shortening and lengthening contractions in vivo," *Journal of Applied Physiology*, Vol. 95, pp. 1090–1096, 2003.

14. Kinugasa, R., D. Shin, J. Yamauchi, C. Mishra, J. Hodgson, V. Edgerton, and S. Sinha, "Phase-contrast mri reveals mechanical behavior of superficial and deep aponeuroses in human medial gastrocnemius during isometric contraction," *J Appl Physiol*, Vol. 105, pp. 1312–1320, 2008.

15. Shin, D., J. Hodgson, V. Edgerton, and S. Sinha, "In vivo intramuscular fascicle-aponeuroses dynamics of the human medial gastrocnemius during plantarflexion and dorsiflexion of the foot," *Journal of Applied Physiology*, Vol. 107, pp. 1276–1284, 2009.

16. Blemker, S., P. Pinsky, and S. Delp, "A 3d model of muscle reveals the causes of nonuniform strains in the biceps brachii," *J Biomech*, Vol. 38, pp. 657–665, 2005.

17. Pappas, G., D. Asakawa, S. Delp, F. Zajac, and J. Drace, "Nonuniform shortening in the biceps brachii during elbow flexion," *J Appl Physiol*, Vol. 92, pp. 2381–2389, 2002.

18. Asakawa, D., S. Blemker, G. Gold, and S. Delp, "In vivo motion of the rectus femoris muscle after tendon transfer surgery," *Journal of Biomechanics*, Vol. 35, pp. 1029–1037, 2002.

19. Damon, B., Z. Ding, A. Anderson, A. Freyer, and J. Gore, "Validation of diffusion tensor mri-based muscle fiber tracking," *Magnetic Resonance in Medicine*, Vol. 48, pp. 97–104, 2002.

20. Van Donkelaar, C., L. Kretzers, P. Bovendeerd, L. Lataster, K. Nicolay, J. Janssen, and M. Drost, "Diffusion tensor imaging in biomechanical studies of skeletal muscle function," *Journal of Anatomy*, Vol. 194, pp. 79–88, 1999.

21. Heemskerk, A., T. Sinha, K. Wilson, Z. Ding, and B. Damon, "Repeatability of dti-based skeletal muscle fiber tracking," *NMR Biomed*, Vol. 23, pp. 294–303, 2010.

22. Drost, M., M. Froeling, P. Oomen, A. Nederveen, and G. Strijkers, "Diffusion tensor mri as tool to determine subject specific muscle architecture," (Leuven–Belgium), IUTAM symposium on human movement analysis and simulation, 2010.

23. Sinha, S., U. Sinha, and V. Edgerton, "In vivo diffusion tensor imaging of the human calf muscle," *J Magn Reson Imaging*, Vol. 24, pp. 182–190, 2006.

24. Heemskerk, A., T. Sinha, K. Wilson, Z. Ding, and B. Damon, "Quantitative assessment of dti-based muscle fiber tracking and optimal tracking parameters," *Magn Reson Med*, Vol. 61, pp. 467–472, 2009.

25. Budzik, J., V. Le Thuc, X. Demondion, M. Morel, D. Chechin, and A. Cotten, "In vivo mr tractography of thigh muscles using diffusion imaging: Initial results," *European Radiology*, Vol. 17, pp. 3079–3085, 2007.

26. Froeling, M., J. Oudeman, S. van den Berg, K. Nicolay, M. Maas, G. Strijkers, M. Drost, and A. Nederveen, "Reproducibility of diffusion tensor imaging in human forearm muscles at 3.0 t in a clinical setting," *Magnetic Resonance in Medicine*, Vol. 64, pp. 1182–1190, 2010.

27. Englund, E., C. Elder, Q. Xu, Z. Ding, and B. Damon, "Combined diffusion and strain tensor mri reveals a heterogeneous, planar pattern of strain development during isometric muscle contraction," *Am J Physiol Regul Integr Comp Physiol*, Vol. 300, pp. 1079–1090, 2011.

28. Felton, S., T. Gaige, T. Benner, R. Wang, T. Reese, V. Wedeen, and R. Gilbert, "Associating the mesoscale fiber organization of the tongue with local strain rate during swallowing," *Journal of Biomechanics*, Vol. 41, pp. 1782–1789, 2008.

29. Huijing, P., "Muscle as a collagen fiber reinforced composite: A review of force transmission in muscle and whole limb," *J Biomech*, Vol. 32, pp. 329–345, 1999.

30. Herbert, P., P. Hoang, and S. Gandevia, "Are muscles mechanically independent?," *Journal of Applied Physiology*, Vol. 104, pp. 1549–1550, 2008.

31. Maas, H., and T. Sandercock, "Force transmission between synergistic skeletal muscles through connective tissue linkages," *J Biomed Biotechnol*, Vol. 2010, p. 575672, 2010.

32. Tidball, J., "Myotendinous junction injury in relation to junction structure and molecular composition," *Exerc Sport Sci Rev*, Vol. 19, pp. 419–445, 1991.

33. Hawkins, D., and M. Bey, "Muscle and tendon force-length properties and their interactions in vivo," *Journal of Biomechanics*, Vol. 30, pp. 63–70, 1997.

34. Huijing, P., "Epimuscular myofascial force transmission: A historical review and implications for new research. international society of biomechanics muybridge award lecture, taipei, 2007," *J Biomech*, Vol. 42, pp. 9–21, 2009.

35. Trotter, J., and P. Purslow, "Functional-morphology of the endomysium in series fibered muscles," *Journal of Morphology*, Vol. 212, pp. 109–122, 1992.

36. Street, S., "Lateral transmission of tension in frog myofibers - a myofibrillar network and transverse cytoskeletal connections are possible transmitters," *Journal of Cellular Physiology*, Vol. 114, pp. 346–364, 1983.

37. Yucesoy, C., G. Baan, B. Koopman, H. Grootenboer, and P. Huijing, "Pre-strained epimuscular connections cause muscular myofascial force transmission to affect properties of synergistic ehl and edl muscles of the rat," *Journal of Biomechanical Engineering-Transactions of the Asme*, Vol. 127, pp. 819–828, 2005.

38. Huijing, P., A. Yaman, C. Ozturk, and C. Yucesoy, "Effects of knee joint angle on global and local strains within human triceps surae muscle: Mri analysis indicating in vivo myofascial force transmission between synergistic muscles," *Surgical and Radiologic Anatomy*, Vol. 33, pp. 869–879, 2011.

39. Huijing, P., and G. Baan, "Myofascial force transmission: Muscle relative position and length determine agonist and synergist muscle force," *Journal of Applied Physiology*, Vol. 94, pp. 1092–1107, 2003.

40. Maas, H., G. Baan, and P. Huijing, "Intermuscular interaction via myofascial force transmission: Effects of tibialis anterior and extensor hallucis longus length on force transmission from rat extensor digitorum longus muscle," *Journal of Biomechanics*, Vol. 34, pp. 927–940, 2001.

41. Maas, H., G. Baan, and P. Huijing, "Muscle force is determined also by muscle relative position: Isolated effects," *Journal of Biomechanics*, Vol. 37, pp. 99–110, 2004.

42. Yucesoy, C., B. Koopman, P. Huijing, and H. Grootenboer, "Three-dimensional finite element modeling of skeletal muscle using a two-domain approach: Linked fiber-matrix mesh model," *J Biomech*, Vol. 35, pp. 1253–1262, 2002.

43. Yucesoy, C., B. Koopman, G. Baan, H. Grootenboer, and P. Huijing, "Effects of inter- and extramuscular myofascial force transmission on adjacent synergistic muscles: Assessment by experiments and finite-element modeling," *Journal of Biomechanics*, Vol. 36, pp. 1797–1811, 2003.

44. Thirion, J., "Image matching as a diffusion process: An analogy with maxwell's demons," *Med Image Anal*, Vol. 2, pp. 243–260, 1998.

45. Yaman, A., C. Ozturk, P. Huijing, and C. Yucesoy, "Magnetic resonance imaging assessment of mechanical interactions between human lower leg muscles in vivo," *J Biomech Eng*, Vol. 135, p. 91003, 2013.

46. Yaman, A., *Mri assessment of in vivo epimuscular myofascial force transmission*. PhD thesis, Bogazici University, Istanbul, Turkey, 2014.

47. Akyazi, P., "Skeletal muscle deformation analysis using diffusion tensor magnetic resonance imaging," Master's thesis, Bogazici University, Istanbul, Turkey, 2013.

48. Pamuk, U., A. Karakuzu, P. Akyazi, B. Acar, C. Oztürk, and C. Yucesoy, "Magnetic resonance imaging analyses confirm so far theoretically posed intermuscular interaction effects, in vivo," (Rome–Italy), The XX congress of the ISEK, 2014.

49. Karakuzu, A., U. Pamuk, C. Ozturk, and C. Yucesoy, "Assessment of in vivo skeletal muscle mechanics using multimodal magnetic resonance imaging based approaches," (Istanbul–Turkey), 18th BIYOMUT, 2014.

50. Huijing, P., and G. Baan, "Myofascial force transmission causes interaction between adjacent muscles and connective tissue: Effects of blunt dissection and compartmental fasciotomy on length force characteristics of rat extensor digitorum longus muscle," *Arch Physiol Biochem*, Vol. 109, pp. 97–109, 2001.

51. Ates, F., Y. Temelli, and C. Yucesoy, "Intraoperative experiments show relevance of inter-antagonistic mechanical interaction for spastic muscle's contribution to joint movement disorder," *Clinical Biomechanics*, Vol. 29, pp. 943–949, 2014.

52. Rainoldi, A., G. Melchiorri, and I. Caruso, "A method for positioning electrodes during surface emg recordings in lower limb muscles," *Journal of Neuroscience Methods*, Vol. 134, pp. 37–43, 2004.

53. Oshita, K., and S. Yano, "Relationship between force fluctuation in the plantar flexor and sustainable time for single-leg standing," *Journal of Physiological Anthropology*, Vol. 29, pp. 89–93, 2010.

54. Weis, J., A. Ericsson, and A. Hemmingsson, "Chemical shift artifact-free imaging: A new option in mri?," *Magnetic Resonance Imaging*, Vol. 16, pp. 839–844, 1998.

55. Sharp, G., N. Kandasamy, H. Singh, and M. Folkert, "Gpu-based streaming architectures for fast cone-beam ct image reconstruction and demons deformable registration," *Physics in Medicine and Biology*, Vol. 52, pp. 5771–5783, 2007.

56. Muyan-Ozcelik, P., J. Owens, J. Xia, and S. Samant, "Fast deformable registration on the gpu: A cuda implementation of demons," *International Conference on Computational Sciences and Its Applications, Proceedings*, pp. 223–233, 2008.

57. Kroon, D., and C. Slump, "Mri modalitiy transformation in demon registration," *2009 Ieee International Symposium on Biomedical Imaging: From Nano to Macro, Vols 1 and 2*, pp. 963–966, 2009.

58. *Review of continuum mechanics*. Available: http://www.colorado.edu/engineering, Accessed on May 2015.

59. Tristan-Vega, A., and S. Aja-Fernandez, "Dwi filtering using joint information for dti and hardi," *Medical Image Analysis*, Vol. 14, pp. 205–218, 2010.

60. Clarke, R., P. Scifo, G. Rizzo, F. Dell'Acqua, G. Scotti, and F. Fazio, "Noise correction on rician distributed data for fibre orientation estimators," *Ieee Transactions on Medical Imaging*, Vol. 27, pp. 1242–1251, 2008.

61. Aja-Fernandez, S., C. Alberola-Lopez, and C. Westin, "Noise and signal estimation in magnitude mri and rician distributed images: A lmmse approach," *Ieee Transactions on Image Processing*, Vol. 17, pp. 1383–1398, 2008.

62. Tench, C., P. Morgan, M. Wilson, and L. Blumhardt, "White matter mapping using diffusion tensor mri," *Magnetic Resonance in Medicine*, Vol. 47, pp. 967–972, 2002.

63. A.B., Y., "Assessing dt-mri tractography results via sampling the fiber tract shape," Master's thesis, Bogazici University, Istanbul, Turkey, 2009.

64. Durusut, E., E. Bozkaya, E. Yagci, and E. Acar, "Vavframe : a new concept in platform design," (Belgrade–Serbia), EUROCON 2005, Nov 22-24 2005.

65. Arsigny, V., P. Fillard, X. Pennec, and N. Ayache, "Log-euclidean metrics for fast and simple calculus on diffusion tensors," *Magn Reson Med*, Vol. 56, pp. 411–421, 2006.

66. Froeling, M., A. Nederveen, D. Heijtel, A. Lataster, C. Bos, K. Nicolay, M. Maas, M. Drost, and G. Strijkers, "Diffusion-tensor mri reveals the complex muscle architecture of the human forearm," *J Magn Reson Imaging*, Vol. 36, pp. 237–248, 2012.

67. Descoteaux, M., R. Deriche, T. Knosche, and A. Anwander, "Deterministic and probabilistic tractography based on complex fibre orientation distributions," *IEEE Trans Med Imaging*, Vol. 28, pp. 269–286, 2009.

68. Chow, R., M. Medri, D. Martin, R. Leekam, A. Agur, and N. McKee, "Sonographic studies of human soleus and gastrocnemius muscle architecture: Gender variability," *Eur J Appl Physiol*, Vol. 82, pp. 236–244, 2000.

69. Fedorov, A., R. Beichel, J. Kalpathy-Cramer, J. Finet, J. Fillion-Robin, S. Pujol, C. Bauer, D. Jennings, F. Fennessy, M. Sonka, J. Buatti, S. Aylward, J. Miller, S. Pieper, and R. Kikinis, "3d slicer as an image computing platform for the quantitative imaging network," *Magn Reson Imaging*, Vol. 30, pp. 1323–1341, 2012.

70. Moglo, K., and A. Shirazi-Adl, "Cruciate coupling and screw-home mechanism in passive knee joint during extension–flexion," *J Biomech*, Vol. 38, pp. 1075–1083, 2005.

71. Wolf, S., and J. Kim, "Morphological analysis of the human tibialis anterior and medial gastrocnemius muscles," *Acta Anat (Basel)*, Vol. 158, pp. 287–295, 1997.

72. Muraoka, T., T. Muramatsu, D. Takeshita, Y. Kawakami, and T. Fukunaga, "Length change of human gastrocnemius aponeurosis and tendon during passive joint motion," *Cells Tissues Organs*, Vol. 171, pp. 260–268, 2002.

73. Yucesoy, C., B. Koopman, H. Grootenboer, and P. Huijing, "Finite element modeling of aponeurotomy: Altered intramuscular myofascial force transmission yields complex sarcomere length distributions determining acute effects," *Biomech Model Mechanobiol*, Vol. 6, pp. 227–243, 2007.

74. Kierszenbaum, A., and L. Tres, *Histology and cell biology : an introduction to pathology*, Elsevier Saunders, 2012.

75. Morgan, D., N. Whitehead, A. Wise, J. Gregory, and U. Proske, "Tension changes in the cat soleus muscle following slow stretch or shortening of the contracting muscle," *J Physiol*, Vol. 522 Pt 3, pp. 503–513, 2000.

76. Willems, M., and P. Huijing, "Heterogeneity of mean sarcomere-length in different fibers - effects on length range of active force production in rat muscle," *European Journal of Applied Physiology and Occupational Physiology*, Vol. 68, pp. 489–496, 1994.

77. Clamann, H., "Motor unit recruitment and the gradation of muscle force," *Physical Therapy*, Vol. 73, pp. 830–843, 1993.

78. Fallentin, N., K. Jorgensen, and E. Simonsen, "Motor unit recruitment during prolonged isometric contractions," *Eur J Appl Physiol Occup Physiol*, Vol. 67, pp. 335–341, 1993.

79. Turkoglu, A., P. Huijing, and C. Yucesoy, "Mechanical principles of effects of botulinum toxin on muscle length-force characteristics: An assessment by finite element modeling," *Journal of Biomechanics*, Vol. 47, pp. 1565–1571, 2014.

80. Ates, F., Y. Temelli, and C. Yucesoy, "Human spastic gracilis muscle isometric forces measured intraoperatively as a function of knee angle show no abnormal muscular mechanics," *Clinical Biomechanics*, Vol. 28, pp. 48–54, 2013.

81. Ates, F., *Mechanics of spastic muscle and effects of treatment techniques : assessments with intraoperative and animal experiments.* PhD thesis, Bogazici University, Istanbul, Turkey, 2013.

82. Ates, F., and C. Yucesoy, "Effects of botulinum toxin type a on non-injected bi-articular muscle include a narrower length range of force exertion and increased passive force," *Muscle and Nerve*, Vol. 49, pp. 866–878, 2014.

83. Yucesoy, C., O. Emre Arikan, and F. Ates, "Btx-a administration to the target muscle affects forces of all muscles within an intact compartment and epimuscular myofascial force transmission," *J Biomech Eng*, Vol. 134, p. 111002, 2012.

84. Turkoglu, A., "Mechanical effects of botulinum toxin treatment on isolated muscle: assessment of theoretical paralyzation patterns via finite element modeling," Master's thesis, Bogazici University, Istanbul, Turkey, 2010.

85. Garrett, W., "Muscle strain injuries," *American Journal of Sports Medicine*, Vol. 24, pp. S2–S8, 1996.

86. Shah, J., B. Shah, and A. Shah, "Pictorial essay: Ultrasonography in 'tennis leg'," *Indian J Radiol Imaging*, Vol. 20, pp. 269–273, 2010.